arXiv:2603.02417v1 [stat.ML] 2 Mar 2026

Fisher-Geometric Diffusion in Stochastic Gradient Descent: Optimal Rates, Oracle Complexity, and Information-Theoretic Limits

Daniel Zantedeschi[1] and Kumar Muthuraman[2]

[1]Muma College of Business, University of South Florida, Tampa, FL, USA,
danielz@usf.edu

[2]McCombs School of Business, University of Texas at Austin, Austin, TX, USA,
kumar.muthuraman@mccombs.utexas.edu

March 4, 2026

Abstract

We develop a Fisher-geometric theory of stochastic gradient descent (SGD) in which mini-batch noise is an intrinsic, loss-induced matrix—not an exogenous scalar variance. Under exchangeable sampling, the mini-batch gradient covariance is pinned down (to leading order) by the projected covariance of per-sample gradients: it equals projected Fisher information for well-specified likelihood losses and the projected Godambe (sandwich) matrix for general M-estimation losses. This identification forces a diffusion approximation with Fisher/Godambe-structured volatility (effective temperature $\tau = \eta/b$) and yields an Ornstein–Uhlenbeck linearization whose stationary covariance is given in closed form by a Fisher–Lyapunov equation. Building on this geometry, we prove matching minimax upper and lower bounds of order $\Theta(1/N)$ for Fisher/Godambe risk under a total oracle budget N; the lower bound holds under a martingale oracle condition (bounded predictable quadratic variation), strictly subsuming i.i.d. and exchangeable sampling. These results imply oracle-complexity guarantees for ε-stationarity in the Fisher dual norm that depend on an intrinsic effective dimension and a Fisher/Godambe condition number rather than ambient dimension or Euclidean conditioning. Experiments confirm the Lyapunov predictions and show that scalar temperature matching cannot reproduce directional noise structure.

Keywords: Stochastic gradient descent; Fisher information; Godambe information; information geometry; diffusion approximation; minimax rates; oracle complexity; batch-size control; simulation optimization

1 Introduction

Stochastic gradient descent (SGD) is the computational workhorse behind a large class of operations research and management science problems, including simulation optimization, large-scale stochastic programming, and data-driven estimation in service and supply-chain systems. In these settings, *sampling effort is a decision variable*: each iterate trades off additional replications (or scenarios) against the number of updates that can be executed under a fixed budget. Several widely observed phenomena depend on this tradeoff: small mini-batches often dominate large batches in wall-clock efficiency; constant-step SGD exhibits steady-state "error floors" and implicit regularization; and plain SGD frequently behaves as if it were curvature-aware despite using only first-order information.

This paper offers a unified account of these phenomena by identifying a structural property of the stochastic-gradient oracle that is often treated as exogenous in stochastic approximation: *mini-batch gradient noise has a loss-induced matrix geometry.* Under exchangeable sampling, the leading-order covariance of the mini-batch average is determined by the population covariance of per-sample gradients projected onto identifiable directions. In likelihood settings this matrix is Fisher information; for general losses it is the corresponding Godambe/sandwich geometry. Once this intrinsic matrix is identified, (i) the diffusion approximation used to analyze constant-step SGD becomes structurally determined, (ii) the natural metric for rates is Fisher/Godambe rather than Euclidean, and (iii) batch size admits principled operations-research (OR) design rules. Our central result is thus an *identification*, not merely a bound: the noise covariance is pinned down by the sampling mechanism, and this single structural fact forces the diffusion coefficient, determines the natural convergence metric, and yields tight oracle-complexity guarantees.

While diffusion analyses of constant-step SGD are classical, most treatments either assume isotropic gradient noise or summarize noise effects through scalar quantities such as trace-level variance or Euclidean error. In contrast, we identify the full matrix geometry of mini-batch noise under exchangeable sampling and show that this structure alone determines the diffusion coefficient, the natural convergence metric, and the resulting oracle complexity. The contribution is therefore structural: the geometry is pinned down by the sampling mechanism itself.

Formally, the paper establishes the following results:

1. **Identification of intrinsic mini-batch noise geometry.** Under exchangeable sampling, the leading-order mini-batch gradient covariance is uniquely determined by the projected covariance of per-sample gradients. In likelihood models this reduces to Fisher information; in general M-estimation it becomes the Godambe matrix. Thus the diffusion coefficient is not a modeling assumption but a structural consequence of the sampling mechanism.

2. **Fisher-structured stationary law.** The induced diffusion admits an Ornstein–Uhlenbeck linearization whose stationary covariance solves a Fisher–Lyapunov equation, yielding closed-

form equilibrium structure and explicit directional variance formulas.

3. **Minimax-optimal Fisher/Godambe risk bounds.** Under a martingale oracle condition (bounded predictable quadratic variation), we prove matching upper and lower bounds of order $\Theta(1/N)$ for Fisher/Godambe risk under a total oracle budget N.

4. **Oracle complexity in intrinsic dimension.** The resulting complexity guarantees for ε-stationarity in the Fisher dual norm depend on an intrinsic effective dimension and a Fisher/Godambe condition number rather than ambient dimension or Euclidean conditioning.

1.1 Motivation: Simulation Optimization as Sampling Control

Consider the canonical simulation-optimization objective

$$\min_{\theta \in \Theta} L(\theta) \;:=\; \mathbb{E}\big[h(\theta, \xi)\big], \tag{1}$$

where ξ denotes random inputs (arrivals, service times, demand shocks) and $h(\theta, \xi)$ is the induced cost. A standard stochastic-gradient estimator uses b simulation replications,

$$g_B(\theta) \;=\; \frac{1}{b} \sum_{i=1}^{b} \nabla_\theta h(\theta, \xi_i), \qquad \xi_i \overset{\text{i.i.d.}}{\sim} P, \tag{2}$$

followed by $\theta^+ = \theta - \eta\, g_B(\theta)$. Classical variance-reduction intuition focuses on the scalar variance of a component or of a scalarized performance measure, suggesting that larger b should always help. In practice, under fixed compute or sample budgets, small b often wins.

The key reason is geometric: the noise in $g_B(\theta)$ is not scalar. Its covariance is a *matrix* that encodes which directions are intrinsically informative and which are weakly identified by the underlying experiment. Our results show that, to leading order, this covariance scales as $b^{-1}G^*(\theta)$, where $G^*(\theta)$ is the projected covariance of per-sample gradients. For likelihood-based objectives, $G^*(\theta)$ reduces to projected Fisher information; for general M-estimation and proper-scoring objectives it is the corresponding Godambe-aligned object. This provides the statistical foundation for interpreting SGD as a controlled diffusion whose "temperature" is $\tau = \eta/b$.

OR problem classes where the theory applies. The sampling-control perspective above is not limited to simulation optimization. Three canonical OR problem classes share the same structure: (i) *simulation optimization* (queuing, inventory, revenue management), where each mini-batch gradient requires b simulation replications and the replication budget is the binding constraint; (ii) *stochastic programming / SAA*, where scenario-based gradient estimates are drawn from an empirical distribution and the number of scenarios per iterate is a design variable subject to a total scenario budget; and (iii) *online M-estimation in service systems*, where per-transaction loss

gradients arrive in a stream and the batch window trades off estimation quality against decision latency. In each case, sampling effort is explicit, b is small relative to d, and the question "how many samples per iterate?" is operationally binding. The theory developed below applies uniformly to all three classes.

1.2 Core Insights

Before turning to formal statements, we summarize the main idea informally. When SGD computes a mini-batch gradient by averaging b per-sample gradients, the resulting noise is not "generic randomness." Its covariance—the matrix describing which directions are noisy and which are quiet—is determined by the loss function and the data-generating process. Specifically, directions in parameter space where the data carry more information (in the sense of Fisher information) naturally produce larger gradient fluctuations.

This has three immediate consequences that do not require any SDE machinery to appreciate:

1. **The noise is structured, not spherical.** If one doubles the batch size, noise is reduced equally in all directions, but the *shape* of the noise ellipsoid is fixed by the statistical problem. This shape is the Fisher information matrix (for likelihood losses) or its generalization, the Godambe matrix (for arbitrary losses).

2. **The right metric for measuring SGD error is statistical, not Euclidean.** Since the noise is Fisher-shaped, measuring convergence in the Fisher metric (which weights directions by their statistical informativeness) gives tighter and more interpretable bounds than the Euclidean metric.

3. **Batch size is a design variable, not just a hyperparameter.** Because batch size controls the "temperature" $\tau = \eta/b$ of a diffusion process, it directly governs the Fisher/Godambe-weighted stationary covariance through the Lyapunov balance. This makes b a first-class design lever: under a fixed sampling budget $N = Tb$, the oracle complexity (Theorem 7.3) scales with the intrinsic dimension d_{eff} and condition number κ_F, clarifying when small batches are near-optimal rather than merely convenient.

The remainder of this section makes these claims precise.

1.3 What We Show

(i) Alignment from sampling theory. Under exchangeable sampling (and simple random mini-batching), the mini-batch gradient satisfies

$$\mathrm{Cov}(g_B(\theta) \mid \mathcal{F}) \;=\; \frac{1}{b}\, G^*(\theta) \;+\; o(b^{-1}), \tag{3}$$

where $G^*(\theta)$ is the projected gradient-noise covariance (Section 4). In particular, for correctly specified likelihood losses $G^*(\theta) = F^\star(\theta)$ (Fisher alignment). *That is, the noise in a mini-batch gradient is not arbitrary—to leading order, it is proportional to the Fisher/Godambe matrix, which encodes how informative the data are about the parameters.*

(ii) Diffusion and Lyapunov structure. In the small-stepsize regime with $\tau = \eta/b$ held fixed, the SGD recursion admits a diffusion approximation whose diffusion covariance is $\tau\, G^*(\theta)$ (Section 5). Near a nondegenerate critical point, the limiting SDE linearizes to an OU process whose stationary covariance Σ_∞ solves the Lyapunov equation

$$H^\star \Sigma_\infty + \Sigma_\infty (H^\star)^\top \;=\; \tau\, G^*(\theta^\star), \tag{4}$$

making explicit that steady-state fluctuations are governed by the ratio of curvature to Fisher/Godambe noise.

(iii) Matching Fisher-metric rates and minimax lower bounds. We analyze SGD performance in the frozen Fisher/Godambe geometry at $\theta^\star$. We prove $1/T$ upper bounds for mean-square error in the Fisher metric and match them with information-theoretic lower bounds (via van Trees), showing the rate and its dependence on the intrinsic geometry are minimax tight (Sections 6 and 7).

(iv) Oracle complexity in statistical rather than Euclidean conditioning. Our oracle complexity bounds scale with a Fisher/Godambe condition number and an effective dimension, isolating statistical difficulty from purely Euclidean conditioning. This clarifies when classical Hessian-based condition numbers can be misleading for statistical objectives.

(v) Batch size as an OR design variable. The framework above connects batch-size design to Fisher/Godambe geometry; Section 9 discusses extensions to misspecification, dependence, and operational effort allocation.

Main Results (informal).

Theorem 4.3 — Mini-batch covariance $= \frac{1}{b}\, G^\star(\theta)$ (Fisher under correct specification).

Theorem 5.4 — SGD $\Rightarrow$ SDE with Fisher/Godambe-structured volatility at temperature $\tau = \eta/b$.

Thm. 5.7, Cor. 5.8 — OU linearization at $\theta^\star$; stationary covariance solves a Lyapunov equation.

Thms. 6.4, 6.8 — Matching $1/(Tb)$ upper and lower bounds in the Fisher metric.

Theorem 7.3 — Oracle complexity $N = \widetilde{\Theta}(\kappa_F\, d_{\text{eff}}/\varepsilon^2)$ for Fisher-dual stationarity.

1.4 Positioning and Organization

Our analysis connects classical stochastic approximation (Robbins and Monro, 1951; Kushner and Yin, 2003) with diffusion views of SGD (Mandt et al., 2017; Li et al., 2017) and information geometry (Amari, 1998), while emphasizing the operations-research-relevant regime where sampling effort is explicit and often $b \ll d$. Unlike diffusion analyses that posit a fixed gradient-noise covariance near stationarity, we derive the covariance structure directly from exchangeable sampling. In our framework, the Fisher/Godambe geometry is not an auxiliary modeling assumption but a consequence of the sampling mechanism itself.

Section 2 reviews related work and positions the contribution. Section 3 defines the oracle model, the geometric objects (G^*, Fisher, Godambe), and the local regularity conditions. Section 4 derives the mini-batch covariance alignment from sampling theory and exchangeability. Section 5 builds the diffusion approximation and local OU/Lyapunov structure on this alignment. Section 6 proves matching upper and lower bounds in Fisher geometry, and Section 7 states oracle complexity in the Fisher/Godambe metric. Section 8 provides numerical validation via two key diagnostics: (i) the Lyapunov/OU stationary risk prediction is accurate—the empirical Fisher-metric risk plateaus at the predicted $\mathrm{Tr}(G^\star H^{-1})$ level; and (ii) scalar temperature matching fails directionally—a rotation sweep reveals cross-covariance structure that no isotropic surrogate can reproduce. Section 9 discusses extensions to misspecification, dependence, and OR-specific design rules.

Reading guide. Readers primarily interested in practical implications may start with Section 7 (oracle complexity) and Section 8 (numerical validation), referring back to Sections 4–5 for the underlying alignment and diffusion theory as needed. Readers interested in the theoretical contributions should follow the paper linearly. The main text includes proofs of all spine results; auxiliary lemmas and concentration tools are collected in the appendices.

2 Literature Review and Positioning

This paper sits at the intersection of stochastic approximation, diffusion approximations for SGD, information geometry, and oracle-complexity theory, with a deliberate focus on operations research settings where sampling effort is an explicit decision variable. In these settings, the mini-batch size b is a budget-constrained design choice: our results convert it into an effective temperature control via the ratio $\tau = \eta/b$, providing actionable design rules for practitioners allocating simulation effort. The unifying thread is that *SGD is a statistical experiment*: the stochastic gradient oracle is generated by sampling, and its noise therefore has an intrinsic geometry determined by the loss and the data model.

To make the contribution transparent, we organize prior work around two recurring degrees of freedom: (i) whether the mini-batch noise covariance is *assumed* (exogenous) or *derived* from the

sampling mechanism; and (ii) whether performance and rates are stated in a Euclidean metric or in a statistically meaningful metric (Fisher/Godambe). Table 1 summarizes the resulting taxonomy of primitives and contrasts, and provides pointers to the corresponding sections and theorems in this paper.

2.1 Stochastic Approximation: Rates with Exogenous Noise Geometry

Classical stochastic approximation studies recursions of the form

$$\theta_{t+1} = \theta_t - \eta_t\{h(\theta_t) + \xi_{t+1}\}, \tag{5}$$

where h is a vector field and ξ_t is a martingale-difference noise process. Under stability and integrability conditions, $\theta_t \to \theta^\star$ with $h(\theta^\star) = 0$, and with additional smoothness one obtains a $\sqrt{t}$-CLT whose covariance is characterized by a Lyapunov equation involving the Jacobian $J(\theta^\star)$ and a long-run noise covariance Γ (Robbins and Monro, 1951; Dvoretzky, 1956; Kushner and Yin, 2003). Optimal finite-time rates under averaging were established by Polyak and Juditsky (1992).

This framework is foundational, but for stochastic gradients it leaves the key object Γ *exogenous*. In SGD, the noise is *endogenous*: it is created by mini-batching and therefore inherits structure from the sampling design and the statistical objective. Our first contribution is to make this structure explicit. As summarized in the first row of Table 1, Theorem 4.3 derives the leading-order covariance of the mini-batch mean from exchangeable sampling (with finite-population correction), identifying the intrinsic matrix $G^\star(\theta)$ (Fisher for likelihood losses, Godambe/sandwich more generally) that governs subsequent diffusion and rate results.

2.2 Diffusion Approximations: Which Diffusion Matrix?

A large literature interprets constant-step SGD as an approximate discretization of an SDE and uses its stationary distribution to explain implicit regularization and generalization behavior (Mandt et al., 2017; Li et al., 2017; Smith et al., 2021). A common template is

$$d\theta_t = -\nabla L(\theta_t)\, dt + \sqrt{2\tau}\, \mathbf{C}(\theta_t)^{1/2} dW_t, \qquad \tau = \eta/b, \tag{6}$$

with multiple proposed specifications for $\mathbf{C}(\theta)$ (isotropic, Hessian-based, Fisher-based, or empirically estimated).

Our results eliminate this modeling degree of freedom in the exchangeable/i.i.d. baseline. As summarized in Table 1, the diffusion matrix is not a free choice: it is implied by the mini-batch design and equals (to leading order) the projected gradient-noise covariance $G^\star(\theta)$; see Theorem 4.3. This pins down the diffusion approximation in Theorem 5.4 and yields a local OU regime with a Lyapunov balance governed by $G^\star$ and temperature $\tau = \eta/b$; see Corollary 5.8.

Contrast with existing diffusion analyses. Mandt et al. (2017) treat the diffusion coefficient as a tunable modeling choice calibrated post hoc; Li et al. (2017) derive modified equations that capture discretization bias but do not identify the covariance with a population-level statistical object; Smith et al. (2021) connect implicit regularization to noise structure but work in a Hessian-scaling regime rather than deriving the matrix from sampling theory. Our contribution is complementary and more primitive: we show that, under standard mini-batch sampling, the diffusion matrix is *forced* to be $G^\star(\theta)$—a quantity determined entirely by the loss and the data model—before any discretization correction or regularization argument is applied. This identification is what enables the subsequent rate-matching bounds (Theorems 6.4–6.8) and the oracle-complexity guarantee (Theorem 7.3) in a statistically natural metric.

2.3 Scaling Regimes and the Small-Batch Operating Region

Recent rigorous diffusion-limit work studies joint regimes in which dimension, batch size, and step size scale together (Paquette et al., 2024). These results provide clean functional CLTs, but typically emphasize settings where b grows proportionally with d.

Our analysis is complementary and closer to operations-research operating constraints. We keep d fixed and treat b as an explicit design variable, with particular attention to the common regime $b \ll d$. In this regime, it is not enough to track a scalar variance level; the *matrix* geometry of $G^\star(\theta)$ controls both transient behavior and risk. This viewpoint feeds directly into Fisher-metric finite-time rates (Section 6) and oracle complexity (Section 7; Theorem 7.3); see Table 1.

2.4 Information Geometry and Natural Gradients

Information geometry treats Fisher information as a Riemannian metric and motivates natural-gradient updates (Amari, 1998; Martens, 2020):

$$\theta_{t+1} = \theta_t - \eta\, F(\theta_t)^{-1} \nabla L(\theta_t). \tag{7}$$

Natural gradients enjoy invariance and improved conditioning, but they require estimating and (approximately) inverting $F(\theta)$.

Our contribution is orthogonal: we identify where intrinsic statistical geometry enters *plain* SGD. The geometry appears implicitly through the *diffusion* term rather than the drift: mini-batch noise injects anisotropic fluctuations aligned with $G^\star(\theta)$, and the local OU equilibrium shows that stationary spread is governed by a Lyapunov balance rooted in the intrinsic statistical geometry (Corollary 5.8). This sharpens the empirical observation that SGD can behave as if it were "curvature-aware" without explicit preconditioning: SGD is not a natural-gradient method, but its noise is naturally shaped.

2.5 Minimax Rates and Information-Theoretic Limits

Lower bounds for stochastic first-order optimization are commonly stated in Euclidean norms under smoothness and strong convexity (Nemirovski et al., 2009; Agarwal et al., 2012). For statistical objectives, such bounds can be loose because Euclidean distance is not the right notion of local distinguishability.

We therefore state both upper and lower bounds in the Fisher/Godambe metric. Using a van Trees (Bayesian Cramér–Rao) argument, we derive a minimax lower bound in Fisher geometry (Theorem 6.8) and match it with a Fisher-Lyapunov upper bound (Theorem 6.4). This identifies the intrinsic drivers of complexity as statistical curvature and dimensionality in the induced metric (e.g., $\lambda_{\min}(F^\star)$ and d_{eff}), as summarized in Table 1.

2.6 Operations Research Context: Sampling Budgets and Effort Allocation

In simulation optimization, stochastic programming, and sample-average approximation (SAA), gradients are estimated from sampled scenarios and sampling cost is explicit (Fu, 2006; Shapiro et al., 2014; Chernoff, 1959). Batch size is therefore not merely a tuning knob: it is a decision variable subject to a budget.

Our framework connects this OR viewpoint to Fisher/Godambe geometry. Because batching controls temperature $\tau = \eta/b$, it directly shapes the diffusion amplitude and hence terminal risk in the appropriate metric. Section 9 outlines how this naturally leads to a covariance-control / effort allocation problem. Table 1 summarizes the positioning of our contributions.

2.7 Why Small Batches Can Work When $b \ll d$

The empirical preference for small batches persists even in very high-dimensional settings (Keskar et al., 2017; Shallue et al., 2019; McCandlish et al., 2018). Our results provide a principled explanation compatible with OR budgeting:

1. **Throughput dominates precision** under fixed sample budgets: N total samples imply $T = N/b$ updates, so smaller b buys more opportunities for contraction.

2. **Geometry governs exploration:** under Fisher/Godambe alignment, noise is anisotropic and concentrates along statistically flat directions, not merely "high variance" in Euclidean units.

3. **Effective dimension can be much smaller than d:** the relevant rates scale with d_{eff} rather than ambient dimension.

4. **Operational constraints are not merely limitations:** practical ceilings on b can be near-optimal when viewed through information-efficiency per unit sampling cost.

Table 1: Positioning: primitives, contrasts, and where each appears in the paper.

Primitive	Status quo	This paper	Pointers
Mini-batch noise covariance	Exogenous / isotropic / heuristic Γ	Derived from sampling: $\mathrm{Cov}(g_B) \propto b^{-1}G^\star(\theta)$; Fisher is a special case	Sec. 4; Thm. 4.3
Diffusion matrix for SGD	Postulated $\mathbf{C}(\theta)$ in SDEs	Diffusion coefficient is forced by sampling theory: $G^\star(\theta)$	Sec. 5; Thm. 5.4
OU / Lyapunov equilibrium	Heuristic OU with ad hoc covariance	OU linearization with Lyapunov balance driven by $G^\star$ at temperature $\tau = \eta/b$	Sec. 5; Cor. 5.8
Metric for rates	Euclidean distance; κ_H dominates	Fisher/Godambe metric is the natural risk	Sec. 6; Thm. 6.4
Lower bounds	Euclidean oracle lower bounds	Information-theoretic lower bound in Fisher metric (van Trees)	Sec. 6; Thm. 6.8
Dimension notion	Ambient d	Effective dimension d_{eff} induced by $F^\star$ / $G^\star$	Sec. 6; Def. (35)
Oracle complexity	Euclidean stationarity; κ_H	Fisher-dual stationarity; κ_F and d_{eff}	Sec. 7; Thm. 7.3

The message is not that smaller batches are always better, but that the right batch size is a function of *statistical geometry and budget*, not only hardware or scalar variance reduction.

Across all of these threads, the contribution of this paper reduces to a single identification—the noise covariance of mini-batch SGD is determined by the loss and the sampling design—from which the diffusion limit, the rate-matching bounds, and the oracle complexity follow as necessary consequences.

3 Problem Setup and Preliminaries

This section fixes notation, specifies the stochastic-gradient oracle, and records the geometric objects that govern the diffusion approximation and the rate/complexity bounds. The perspective is *Mathematics of Operations Research*: we make the sampling design explicit, separate intrinsic noise geometry from finite-population correction, and state the local regularity conditions used throughout.

3.1 Notation and macros used throughout

We work on a measurable space $(\mathcal{Z}, \mathcal{A})$. Vectors use the Euclidean inner product $\langle u, v\rangle = u^\top v$ and norm $\|u\|_2$. For a symmetric matrix A, $\|A\|_{\mathrm{op}}$ denotes the operator norm and $\lambda_{\min}(A), \lambda_{\max}(A)$ its extreme eigenvalues.

3.2 Data model, objective, and stochastic-gradient oracle

Let $\Theta \subseteq \mathbb{R}^d$ be open and convex. Let Q denote the (unknown) data distribution on $(\mathcal{Z}, \mathcal{A})$, and let $\ell : \Theta \times \mathcal{Z} \to \mathbb{R}$ be a measurable loss. Define the population risk

$$L(\theta) \;:=\; \mathbb{E}_{Z\sim Q}\big[\ell(\theta; Z)\big], \tag{8}$$

and let $\theta^\star \in \arg\min_{\theta\in\Theta} L(\theta)$ be a (local) minimizer.

Finite-population sampling model. We observe a dataset $z_{1:n} := (z_1, \ldots, z_n)$ drawn i.i.d. from Q (or, in the exchangeability formulation of Section 4, conditionally i.i.d. given a directing measure). All lower bounds in Section 6 are stated for a general oracle transcript with bounded predictable information (Assumption 6.6); the i.i.d. sampling model is recovered as a special case. At iteration t, the algorithm selects a mini-batch $B_t \subseteq \{1, \ldots, n\}$ of size b_t uniformly *without replacement* and forms the mini-batch gradient

$$g_t(\theta) \;:=\; \frac{1}{b_t}\sum_{i\in B_t} \psi(\theta; z_i), \qquad \psi(\theta; z) := \nabla_\theta \ell(\theta; z). \tag{9}$$

The SGD recursion is

$$\theta_{t+1} \;=\; \theta_t - \eta_t\, g_t(\theta_t), \tag{10}$$

with stepsize $\eta_t > 0$.

Filtration and martingale structure. Let $\mathcal{F}_t$ be the σ-field generated by $(\theta_0, B_0, \ldots, B_{t-1}, \theta_t)$ and the dataset $z_{1:n}$. Then

$$\xi_t(\theta_t) := g_t(\theta_t) - \mathbb{E}[g_t(\theta_t) \mid \mathcal{F}_t]$$

is a martingale difference sequence with respect to $(\mathcal{F}_t)$, and all diffusion limits are driven by the predictable quadratic variation of $\sum_t \eta_t \xi_t$.

Cost accounting (oracle calls). We measure computational cost in *sample-gradient evaluations*. One iteration with batch size b_t uses b_t sample evaluations. After T iterations, the total sampling budget is

$$N_T \;:=\; \sum_{t=0}^{T-1} b_t. \tag{11}$$

We report results both in iterations T and in oracle calls N_T, since the control/OR questions in naturally optimize over batch allocation under a fixed N_T.

3.3 Likelihood losses: Fisher information and the induced metric

When $\ell(\theta; z) = -\log p_\theta(z)$ for a parametric family $\{P_\theta : \theta \in \Theta\}$ with density p_θ, the score is $s_\theta(z) := \nabla_\theta \log p_\theta(z)$ and the loss gradient is the negative score, $\nabla_\theta \ell(\theta; z) = -s_\theta(z)$. The intrinsic noise geometry reduces to Fisher information.

Definition 3.1 (Fisher information)**.** Assume p_θ is differentiable in θ and $s_\theta(Z)$ is square integrable under P_θ. The Fisher information is

$$F(\theta) \;:=\; \mathbb{E}_\theta\big[s_\theta(Z)s_\theta(Z)^\top\big]. \tag{12}$$

Lemma 3.2 (Score identities (Lehmann and Casella, 1998, Ch. 7))**.** *Assume $\int p_\theta(z)\,dz = 1$ and differentiation under the integral is valid. Then (i) $\mathbb{E}_\theta[s_\theta(Z)] = 0$ and (ii)*

$$F(\theta) \;=\; -\mathbb{E}_\theta\big[\nabla_\theta^2 \log p_\theta(Z)\big]. \tag{13}$$

Proof. Differentiate $\int p_\theta(z)\,dz = 1$ to obtain $0 = \int \nabla_\theta p_\theta(z)\,dz = \int p_\theta(z)s_\theta(z)\,dz$. For (ii), differentiate $\mathbb{E}_\theta[s_\theta(Z)] = 0$ and use the identity $\nabla_\theta \mathbb{E}_\theta[f(Z)] = \mathbb{E}_\theta[\nabla_\theta f(Z) + f(Z)s_\theta(Z)^\top]$ with $f = s_\theta$. □

Fisher metric. If $F(\theta) \succ 0$, it defines the local inner product $\langle u, v\rangle_{F(\theta)} := u^\top F(\theta) v$ and norm $\|u\|_{F(\theta)} := \sqrt{u^\top F(\theta) u}$. On compact sets where $F(\theta)$ is bounded and bounded away from 0, Fisher and Euclidean norms are equivalent.

3.4 General losses: sandwich / Godambe geometry

For a general loss, information equality need not hold. The relevant local geometry splits into (i) curvature of the drift and (ii) covariance of the estimating equation (gradient).

Definition 3.3 (Noise covariance, sensitivity, and Godambe information)**.** Let $\psi(\theta; z) := \nabla_\theta \ell(\theta; z)$ and define

$$G(\theta) := \mathrm{Cov}\big(\psi(\theta; Z)\big), \tag{14}$$

$$H(\theta) := \nabla^2 L(\theta) \;=\; \mathbb{E}[\nabla_\theta \psi(\theta; Z)]\,, \tag{15}$$

where expectations are under $Z \sim Q$. When $H(\theta)$ is invertible on the identifiable directions, the classical sandwich covariance and Godambe information are

$$\Sigma_{\mathrm{sand}}(\theta) := H(\theta)^{-1} G(\theta) H(\theta)^{-1}, \qquad J_{\mathrm{God}}(\theta) := \Sigma_{\mathrm{sand}}(\theta)^{-1} = H(\theta)^\top G(\theta)^{-1} H(\theta). \tag{16}$$

Remark 3.4 (Likelihood as a special case). If $\ell(\theta; z) = -\log p_\theta(z)$ and the model is correctly specified, then $\psi = s_\theta$ and $G(\theta) = H(\theta) = F(\theta)$ at $\theta^\star$, so the sandwich collapses and the Godambe geometry equals Fisher.

3.5 Projection onto identifiable directions

Projection is only needed when the parametrization is redundant or when only a lower-dimensional tangent space is identifiable.

Definition 3.5 (Tangent-space projection and projected geometry)**.** Let $T_\theta \subseteq \mathbb{R}^d$ denote the identifiable tangent space at θ (i.e., the linear span of directions along which the loss varies at first order; formally $T_\theta := \mathrm{range}(H(\theta))$, or equivalently $\mathrm{supp}(F(\theta))$ in the likelihood case), and let Π_θ be the Euclidean-orthogonal projector onto T_θ. Define the projected noise covariance

$$G^\star(\theta) \;:=\; \Pi_\theta\, G(\theta)\, \Pi_\theta^\top, \tag{17}$$

and, in the likelihood case, the projected Fisher information

$$F^\star(\theta) \;:=\; \Pi_\theta\, F(\theta)\, \Pi_\theta^\top. \tag{18}$$

When $T_\theta = \mathbb{R}^d$, $\Pi_\theta = I$ and $G^\star = G$, $F^\star = F$.

Remark 3.6 (Terminological convention: "Fisher/Godambe"). Throughout the paper we write "Fisher/Godambe" as shorthand for the following identification: in the correctly specified likelihood case, $G^\star(\theta^\star) = F^\star(\theta^\star)$ (Fisher information); for general losses, $G^\star(\theta^\star)$ is the projected gradient covariance whose inverse is the Godambe information. Every theorem statement holds with $G^\star$ in the general case and specializes to $F^\star$ under correct specification. When we write "Fisher metric" or "Fisher-dual norm," the general-loss reader should substitute the corresponding Godambe/sandwich object.

Remark 3.7 (What enters later sections). Sections 4–5 show that the mini-batch noise covariance is (up to a sampling-design factor) exactly $G^\star(\theta)/b_t$ and reduces to $F^\star(\theta)/b_t$ under correct specification. This is the only matrix that enters the diffusion coefficient and Lyapunov balance.

3.6 Local regularity conditions

All results are local near $\theta^\star$ and use standard smoothness/moment and nondegeneracy conditions.

Assumption 3.8 (Smoothness and moments)**.** The loss $\ell(\theta; z)$ is twice continuously differentiable in θ. There exist constants $M < \infty$ and $m_4 < \infty$ such that for all θ in a neighborhood $\mathcal{N}$ of $\theta^\star$:

(a) $\|\nabla_\theta^2 \ell(\theta; z)\|_{\mathrm{op}} \le M$ almost surely;

(b) $\mathbb{E}[\|\psi(\theta; Z)\|_2^4] \le m_4$.

Assumption 3.9 (Local stability)**.** The population risk is locally strongly convex at $\theta^\star$:

$$H^\star := \nabla^2 L(\theta^\star) \succeq \mu I \quad \text{for some } \mu > 0. \tag{19}$$

Assumption 3.10 (Geometric nondegeneracy)**.** The intrinsic noise geometry is positive definite on identifiable directions:

$$G^\star(\theta^\star) \succeq \lambda_{\min} I \quad \text{for some } \lambda_{\min} > 0. \tag{20}$$

(In the correctly specified likelihood case this is $F^\star(\theta^\star) \succ 0$.)

Remark 3.11 (What these assumptions buy us). Assumption 3.8 ensures uniform Taylor control and moment bounds for the martingale noise. Assumption 3.9 gives a locally stable equilibrium and enables Lyapunov drift arguments. Assumption 3.10 ensures the diffusion coefficient is nondegenerate on identifiable directions and that Fisher/Godambe norms yield meaningful local rates.

4 Fisher/Godambe Alignment of Mini-Batch Noise

Mini-batch gradient noise is *not* an arbitrary covariance: it is pinned down by (i) the sampling design used to form mini-batches and (ii) the intrinsic covariance of the per-sample estimating equation $\psi(\theta; Z)$ (Fisher in the well-specified likelihood case, Godambe noise more generally). We make this precise in two steps:

- an *exact* finite-population identity conditional on the realized dataset (classical survey-sampling algebra), and
- an *exchangeable/i.i.d.* limit that converts the dataset-dependent quantity into the population covariance $G(\theta) := \mathrm{Cov}(\psi(\theta; Z))$ (or its projected analogue).

4.1 Finite-population covariance identity (exact, conditional on data)

Fix θ and condition on the realized dataset $\{z_1, \dots, z_n\}$. Write $\psi_i := \psi(\theta; z_i)$ and define the finite-population mean and covariance

$$\bar{\psi}_n(\theta) := \frac{1}{n}\sum_{i=1}^n \psi_i, \qquad S_n(\theta) := \frac{1}{n-1}\sum_{i=1}^n (\psi_i - \bar{\psi}_n)(\psi_i - \bar{\psi}_n)^\top.$$

Let B be a simple random sample without replacement of size b from $\{1, \dots, n\}$ and define the mini-batch average

$$g_B(\theta) := \frac{1}{b}\sum_{i \in B} \psi_i.$$

Lemma 4.1 (Exact finite-population covariance of the mini-batch mean)**.** *Conditionally on the dataset,*

$$\mathrm{Cov}\big(g_B(\theta) \mid z_{1:n}\big) \;=\; \frac{1}{b}\Big(1-\frac{b}{n}\Big)\, S_n(\theta). \tag{21}$$

Proof. Write $g_B(\theta) = \frac{1}{b}\sum_{i=1}^{n} I_i\,\psi_i$ where $I_i = \mathbf{1}\{i \in B\}$. Under simple random sampling without replacement, $\mathbb{E}[I_i] = b/n$, $\mathrm{Var}(I_i) = \frac{b}{n}(1-\frac{b}{n})$, and for $i \neq j$, $\mathrm{Cov}(I_i, I_j) = -\frac{b(n-b)}{n^2(n-1)}$. Expanding $\mathrm{Cov}(\sum_i I_i\psi_i \mid z_{1:n})$ and collecting terms yields (21). □

Remark 4.2 (Equivalent correction-factor forms). Using S_n with the $1/(n-1)$ normalization gives the factor $(1-b/n)$. If instead one uses the $1/n$ covariance normalization, the factor becomes $1-(b-1)/(n-1)$. The two are algebraically equivalent up to the change of normalization.

Lemma 4.1 is the clean MOR-style decomposition: *sampling design* contributes the scalar finite-population correction $1-b/n$, while the *geometry* lives in $S_n(\theta)$.

4.2 From exchangeability to Godambe/Fisher alignment (population geometry)

We now convert the dataset-dependent covariance $S_n(\theta)$ into a population-level object.

Let $(Z_i)_{i\geq 1}$ be exchangeable with de Finetti directing measure μ (Hewitt and Savage, 1955). Conditional on μ, the sequence is i.i.d. with law P_μ. Define the population covariance (conditional on μ)

$$G_\mu(\theta) \;:=\; \mathrm{Cov}_\mu\big(\psi(\theta; Z)\big), \qquad Z \sim P_\mu, \tag{22}$$

and, when identifiability requires it, the projected version $G^\star_\mu(\theta) := \Pi_\theta G_\mu(\theta)\Pi_\theta^\top$.

Theorem 4.3 (Godambe alignment under exchangeability)**.** *Assume* $\mathbb{E}_\mu\|\psi(\theta;Z)\|_2^2 < \infty$. *Let* $g_B(\theta) = \frac{1}{b}\sum_{i\in B}\psi(\theta; Z_i)$ *where* B *is a uniform subset of* $\{1,\dots,n\}$ *of size* b *(sampling without replacement). Then, conditional on* μ*,*

$$\mathrm{Cov}\big(g_B(\theta) \mid \mu\big) \;=\; \frac{1}{b}\, G_\mu(\theta). \tag{23}$$

Interpretation. *Equation* (23) *is exact (not an approximation) when one marginalizes over both the mini-batch index* B and *the dataset realization conditional on* μ*. The finite-population correction* $(1-b/n)$ *of Lemma 4.1 is present when one conditions on a fixed dataset, but it disappears at the population level because the randomness of the dataset itself contributes a complementary term through the total-covariance decomposition. Equation* (24) *below makes this bookkeeping explicit.*

Moreover,

$$\mathbb{E}\Big[\mathrm{Cov}(g_B(\theta) \mid Z_{1:n}, \mu) \,\big|\, \mu\Big] \;=\; \frac{1}{b}\Big(1-\frac{b}{n}\Big)\,\mathbb{E}[S_n(\theta) \mid \mu] \;=\; \frac{1}{b}\Big(1-\frac{b}{n}\Big)\, G_\mu(\theta), \tag{24}$$

and the remaining part of (23) *comes from the randomness of the dataset through the total-covariance decomposition.*

Proof. Conditional on μ, the sequence $(Z_i)_{i\geq 1}$ is i.i.d. with law P_μ; therefore any uniformly sampled subset of size b has the same joint distribution as the first b coordinates. Hence selecting indices B without replacement from $\{1, \ldots, n\}$ is distributionally equivalent to taking the first b terms, and $g_B(\theta)$ is the average of b i.i.d. draws from P_μ. This yields $\mathrm{Cov}(g_B(\theta) \mid \mu) = \frac{1}{b} G_\mu(\theta)$, proving (23).

For (24), apply the exact identity Lemma 4.1 conditional on $(Z_{1:n}, \mu)$ and take $\mathbb{E}[\cdot \mid \mu]$. Under $\mathbb{E}_\mu \|\psi\|^2 < \infty$, $\mathbb{E}[S_n(\theta) \mid \mu] = G_\mu(\theta)$ (the $1/(n-1)$ sample-covariance normalization is unbiased). □

Remark 4.4 (What "alignment" means operationally). Equation (23) is the alignment statement used by the diffusion/Lyapunov analysis: *mini-batch noise has covariance $\frac{1}{b}$ times a population matrix determined by the loss and the data law.* The finite-population correction in Lemma 4.1 matters when one conditions on a fixed dataset and reuses it many times; in the standard stochastic-approximation regime with fresh randomness across iterations, the population covariance (23) is the relevant object.

Remark 4.5 (Independence structure and finite-dataset reuse). Three conditioning levels should be distinguished: (i) *conditional on the dataset $z_{1:n}$*: mini-batch covariance is $\frac{1}{b}(1 - \frac{b}{n})\, S_n(\theta)$ (Lemma 4.1), with the finite-population correction $(1 - b/n)$ reflecting sampling without replacement from a fixed pool; (ii) *conditional on the directing measure μ*: mini-batch covariance is $\frac{1}{b}\, G_\mu(\theta)$ (Theorem 4.3), with no correction, because the dataset itself is random; (iii) *population level*: the unconditional covariance integrates over μ and dataset randomness, and equals $\frac{1}{b}\, G(\theta)$ under identifiability. The alignment result (23) is *iteration-wise* under fresh sampling: at each iteration t, the mini-batch B_t is drawn independently of previous batches conditional on μ. When a finite dataset is reused across iterations (i.e., without-replacement sampling from the same $z_{1:n}$ at every step), the conditional covariance acquires the standard finite-population correction $(1 - b/n)$. This correction is negligible whenever $b = o(n)$, which is the typical stochastic-approximation regime. It is the population covariance $\frac{1}{b}\, G_\mu(\theta)$ that enters the diffusion approximation (Section 5) and all subsequent rate and complexity results.

Remark 4.6 (Batch size rescales temperature, not geometry). Equation (23) implies that increasing the batch size b rescales the effective temperature $\tau = \eta/b$ (Section 5) but does *not* alter the noise ellipsoid: its shape is entirely determined by the statistical geometry $G_\mu(\theta)$. This decoupling—scale from the sampling budget, shape from the loss—is the operational insight that drives all subsequent rate and complexity results.

Remark 4.7 (Specialization to Fisher alignment). If $\ell(\theta; z) = -\log p_\theta(z)$ and the model is correctly specified, then $\psi(\theta; z) = s_\theta(z)$ is the score and the Bartlett identity yields $\mathrm{Cov}(s_\theta(Z)) = F(\theta)$ at $\theta = \theta^\star$. Projecting onto the identifiable tangent space gives $G^\star_\mu(\theta^\star) = F^\star(\theta^\star)$. Thus (23) becomes $\mathrm{Cov}(g_B(\theta^\star) \mid \mu) = \frac{1}{b} F^\star(\theta^\star)$, i.e., Fisher alignment.

Remark 4.8 (No Gaussian assumption). Neither Lemma 4.1 nor Theorem 4.3 assumes Gaussian noise. Gaussianity enters later only as a *diffusion approximation* (martingale CLT) when we pass

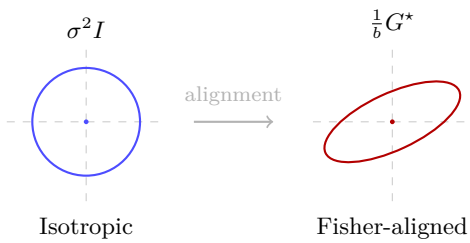

Figure 1: Isotropic noise (left) vs. Fisher-aligned noise (right) at the same total variance. Batch size rescales temperature but not shape.

from the discrete recursion to an OU limit.

Implication for later sections. The analysis in Section 5 depends on a single intrinsic matrix $G^\star(\theta^\star)$ (which equals $F^\star(\theta^\star)$ in the well-specified likelihood case; see Remark 3.6). Once this matrix is fixed, the OU diffusion coefficient, Lyapunov balance, and Fisher-metric rates follow mechanically.

5 Continuous-Time Diffusion Approximation and the OU Regime

This section links the discrete-time SGD recursion to a continuous-time SDE whose diffusion term is *not arbitrary*: its covariance is determined by the mini-batch sampling model and the intrinsic noise geometry derived in Section 4. Specifically, $G^\star(\theta)$ was defined in Section 3 and shown in Theorem 4.3 to govern the leading-order mini-batch covariance. Near a nondegenerate critical point, the SDE linearizes to an Ornstein–Uhlenbeck (OU) process, and its stationary covariance is characterized by a Lyapunov equation. The resulting "temperature" parameter $\tau = \eta/b$ is the scalar that converts sampling effort into diffusion strength. Diffusion approximations are a standard tool in OR for reducing complex stochastic systems to tractable Brownian models (Harrison, 1985; Whitt, 2002); the present setting is analogous, with the sampling mechanism playing the role of the arrival process.

The stationary covariance and risk expressions derived below depend only on the local second-moment structure of the oracle noise and do not require independence across oracle calls; a martingale-difference oracle (Assumption 6.6) suffices.

5.1 SGD decomposition and effective temperature

Fix constant stepsize $\eta > 0$ and batch size b. Let

$$h(\theta) := \nabla L(\theta) = \mathbb{E}[\psi(\theta; Z)], \qquad \psi(\theta; z) := \nabla_\theta \ell(\theta; z),$$

and write the mini-batch gradient estimator as

$$g_t(\theta_t) = h(\theta_t) + \xi_t(\theta_t), \qquad \mathbb{E}[\xi_t(\theta_t) \mid \mathcal{F}_t] = 0,$$

where $\mathcal{F}_t$ is the natural filtration. Then SGD is

$$\theta_{t+1} = \theta_t - \eta\, h(\theta_t) - \eta\, \xi_t(\theta_t). \tag{25}$$

By Theorem 4.3 (and its Fisher specialization in Remark 4.7), the conditional covariance of the noise obeys

$$\mathrm{Cov}(\xi_t(\theta) \mid \mathcal{F}_t) = \frac{1}{b}\, G^\star(\theta) + r_{b,n}(\theta), \qquad \|r_{b,n}(\theta)\|_{\mathrm{op}} = o(b^{-1}) + O(n^{-1}), \tag{26}$$

uniformly in a local neighborhood (the $O(n^{-1})$ term accounts for finite-population corrections and covariance-estimation bias; it is negligible whenever $b = o(n)$).

We call $\tau := \eta/b$ the *effective temperature*:

$$\tau := \eta/b, \tag{27}$$

which will appear as the single scalar factor multiplying the diffusion covariance in the continuous-time limit.

5.2 A diffusion approximation (Euler–Maruyama viewpoint)

Let $s = t\eta$ denote *algorithmic time* and define the piecewise-linear interpolation $\bar{\theta}^\eta(\cdot)$ by $\bar{\theta}^\eta(t\eta) = \theta_t$ and linearity on $[t\eta, (t+1)\eta]$.

Assumption 5.1 (Local regularity and localization)**.** On a neighborhood $\mathcal{U}$ of $\theta^\star$:

(i) $h(\theta) := \nabla L(\theta)$ is locally Lipschitz;

(ii) $\nabla^2 L(\theta)$ is locally Lipschitz (i.e., there exists $L_H < \infty$ such that $\|\nabla^2 L(\theta) - \nabla^2 L(\theta')\|_{\mathrm{op}} \le L_H \|\theta - \theta'\|_2$ for all $\theta, \theta' \in \mathcal{U}$);

(iii) $\sup_{\theta \in \mathcal{U}} \mathbb{E}\|\psi(\theta; Z)\|^4 < \infty$ (bounded fourth moment; implied by Assumption 3.8(b));

(iv) $H^\star := \nabla^2 L(\theta^\star) \succ 0$ (local strong convexity; Assumption 3.9);

(v) for each fixed horizon $T > 0$, $\Pr(\theta_t \in \mathcal{U}\ \forall\, t \le T/\eta) \to 1$ as $\eta \downarrow 0$ (localization; standard in stochastic approximation).

Assumption 5.2 (Asymptotic conditional covariance and Lindeberg)**.** Uniformly on $\mathcal{U}$, $\mathrm{Cov}(\xi_t(\theta) \mid \mathcal{F}_t) = b^{-1} G^\star(\theta) + o(b^{-1})$ and the conditional Lindeberg condition holds for the martingale increments $\eta \xi_t(\theta_t)$ (e.g., via a conditional CLT under exchangeability as in Section 4).

Remark 5.3 (Verifiable sufficient conditions). Assumption 5.2 is implied by the following checkable conditions: (a) $\sup_{\theta\in\mathcal{U}} \mathbb{E}[\|\psi(\theta;Z)\|_2^{2+\delta}] < \infty$ for some $\delta > 0$ (guaranteed by Assumption 3.8(b) with $\delta = 2$); (b) $G^\star(\theta)$ is continuous on $\mathcal{U}$; and (c) the mini-batch is drawn by simple random sampling without replacement from an exchangeable sequence. Under (a)–(c), the conditional Lindeberg condition follows from Lyapunov's criterion applied to the triangular array of centered per-sample gradients, and the covariance identity follows from Theorem 4.3.

Theorem 5.4 (Diffusion approximation)**.** *Suppose Assumptions 5.1–5.2 hold. For fixed batch size $b \geq 1$ and constant step size $\eta > 0$, define the effective temperature $\tau := \eta/b$. For sufficiently small η, the SGD recursion admits a diffusion approximation: the piecewise-linear interpolation $\bar{\theta}^\eta(\cdot)$ converges weakly on $D([0,T];\mathbb{R}^d)$ as $\eta \downarrow 0$ to the solution $\theta(\cdot)$ of the SDE*

$$d\theta_s = -h(\theta_s)\,ds + \sqrt{\tau}\,C^\star(\theta_s)\,dW_s, \qquad C^\star(\theta)\,C^\star(\theta)^\top = G^\star(\theta), \tag{28}$$
$$\text{where } C^\star \text{ is, e.g., the symmetric PSD square root of } G^\star,$$

where W_s is standard d-dimensional Brownian motion. In particular, the diffusion has instantaneous covariance $\tau\,G^\star(\theta_s)\,ds$. In the likelihood / correct-specification case, $G^\star(\theta) = F^\star(\theta)$, so the diffusion covariance is Fisher-structured.

Proof. **Step 1 (scaled interpolation).** Write the recursion in signed-noise form $\theta_{t+1} = \theta_t - \eta h(\theta_t) + \eta\,\zeta_{t+1}$ with $\zeta_{t+1} := -\xi_t$, so $(\zeta_{t+1}, \mathcal{F}_{t+1})$ is a martingale difference. Define the piecewise-linear interpolation $\bar{\theta}^\eta(s)$ on algorithmic time $s = t\eta$ by $\bar{\theta}^\eta(t\eta) = \theta_t$ with linear interpolation.

Step 2 (drift convergence). By local Lipschitzness of h (Assumption 5.1) and the localization condition, $\sum_{k<s/\eta} \eta\,h(\theta_k) \to \int_0^s h(\theta(u))\,du$ uniformly on compacts, by standard ODE-approximation theory (Kushner and Yin, 2003, Chapter 5).

Step 3 (predictable quadratic variation). Define $M^\eta(s) := \sum_{k<s/\eta} \eta\,\zeta_{k+1}$. By the alignment theorem (Theorem 4.3), $\mathbb{E}[\zeta_{k+1}\zeta_{k+1}^\top \mid \mathcal{F}_k] = \frac{1}{b}\,G^\star(\theta_k) + R_k$ with $\|R_k\|_{\mathrm{op}} \leq (c/b)\rho_k$ and $\rho_k \to 0$ locally. Using $\eta^2/b = \eta\tau$:

$$\langle M^\eta\rangle(s) = \sum_{k<s/\eta} \eta^2 \mathbb{E}[\zeta_{k+1}\zeta_{k+1}^\top \mid \mathcal{F}_k] = \tau \sum_{k<s/\eta} \eta\,G^\star(\theta_k) + o(1) \;\to\; \tau\int_0^s G^\star(\theta(u))\,du$$

in probability, uniformly on $[0,S]$.

Step 4 (Lindeberg condition). Assumption 3.8(b) gives $\mathbb{E}[\|\zeta_{k+1}\|^4 \mid \mathcal{F}_k] \leq C m_4/b^2$. Markov's inequality then yields $\sum_{k<S/\eta} \mathbb{E}[\|\eta\zeta_{k+1}\|^2 \mathbf{1}\{\|\eta\zeta_{k+1}\| > \varepsilon\} \mid \mathcal{F}_k] \leq CS\eta^3 m_4/(\varepsilon^2 b^2) \to 0$, verifying the conditional Lindeberg condition.

Step 5 (tightness). Tightness of $\{\bar{\theta}^\eta\}$ in $D([0,S];\mathbb{R}^d)$ follows from Aldous' criterion: drift increments are Lipschitz-controlled and $\mathbb{E}[\|\bar{\theta}^\eta(t+\delta) - \bar{\theta}^\eta(t)\|^2] \leq C\delta$.

Step 6 (martingale FCLT). By the martingale central limit theorem (Ethier and Kurtz, 1986, Theorem 7.1.4), $M^\eta(\cdot) \Rightarrow M(\cdot)$ weakly in $D([0,S];\mathbb{R}^d)$ where M is a continuous martingale

with quadratic variation $\tau \int_0^s G^\star(\theta(u))\,du$. Lévy's characterization gives a Brownian motion W such that $M(s) = \int_0^s \sqrt{\tau}\, C^\star(\theta(u))\,dW_u$. Combining drift and martingale convergence identifies the limit as the unique solution of (28). □

Remark 5.5. The SDE (28) should be read as an Euler–Maruyama limit: SGD is an Euler discretization of a diffusion whose covariance is proportional to the *intrinsic* gradient-noise geometry $G^\star(\theta)$, with overall scale set by the temperature $\tau = \eta/b$.

5.3 The OU regime near a nondegenerate critical point

Assume $\theta^\star$ is a stationary point: $h(\theta^\star) = 0$, and define the local curvature $H^\star := \nabla h(\theta^\star) = \nabla^2 L(\theta^\star)$. Let $\Delta_s := \theta_s - \theta^\star$ denote the centered diffusion.

Assumption 5.6 (Nondegeneracy at $\theta^\star$)**.** $H^\star \succ 0$ and $G^\star(\theta^\star) \succ 0$.

Theorem 5.7 (OU linearization)**.** *Under Assumption 5.6 and the conditions of Theorem 5.4, the diffusion* (28) *admits the local expansion*

$$d\Delta_s = -H^\star \Delta_s\,ds + \sqrt{\tau}\, C^\star(\theta^\star)\,dW_s + \rho_1(\Delta_s)\,ds + \sqrt{\tau}\,\rho_2(\Delta_s)\,dW_s, \tag{29}$$

where $\|\rho_1(\Delta)\| = o(\|\Delta\|)$ *and* $\|\rho_2(\Delta)\|_{\mathrm{op}} = o(1)$ *as* $\Delta \to 0$*. Neglecting the higher-order remainder terms yields the OU SDE*

$$d\Delta_s = -H^\star \Delta_s\,ds + \sqrt{\tau}\, C^\star(\theta^\star)\,dW_s, \qquad C^\star(\theta^\star) C^\star(\theta^\star)^\top = G^\star(\theta^\star). \tag{30}$$

Proof. A Taylor expansion gives $h(\theta^\star + \Delta) = H^\star \Delta + r(\Delta)$ with $\|r(\Delta)\| = o(\|\Delta\|)$. Continuity of $G^\star$ implies we can choose a continuous square root $C^\star(\theta)$ locally (e.g., the symmetric PSD square root), so

$$C^\star(\theta^\star + \Delta) = C^\star(\theta^\star) + R_C(\Delta), \qquad \|R_C(\Delta)\|_{\mathrm{op}} = o(1) \quad (\Delta \to 0).$$

Substituting into (28) and collecting terms yields (29) with $\rho_1(\Delta) := -r(\Delta)$ and $\rho_2(\Delta) := R_C(\Delta)$. □

Corollary 5.8 (Stationary covariance and the Lyapunov equation)**.** *If* $H^\star \succ 0$*, the OU process* (30) *is ergodic with stationary law* $\mathcal{N}(0, \Sigma_\infty)$*. Since* $H^\star \succ 0$*, the matrix* $-H^\star$ *is Hurwitz, so the continuous Lyapunov equation*

$$H^\star \Sigma_\infty + \Sigma_\infty (H^\star)^\top = \tau\, G^\star(\theta^\star) \tag{31}$$

admits a unique symmetric positive definite solution Σ_∞*. In particular, the stationary covariance scales linearly with temperature* $\tau = \eta/b$*.*

Because $H^\star$ is symmetric positive definite, left-multiplying (31) by $(H^\star)^{-1}$ and taking traces gives the trace identity

$$\mathrm{Tr}(\Sigma_\infty) + \mathrm{Tr}\big((H^\star)^{-1}\Sigma_\infty H^\star\big) = \tau\,\mathrm{Tr}\big((H^\star)^{-1}G^\star(\theta^\star)\big), \tag{32}$$

which reduces to $2\,\mathrm{Tr}(\Sigma_\infty) = \tau\,\mathrm{Tr}(G^\star H^{\star-1})$ when $H^\star$ and Σ_∞ commute (e.g., when the eigenbases of curvature and noise align).

Proof. Write $B := \sqrt{\tau}\,(G^\star(\theta^\star))^{1/2}$, so $BB^\top = \tau G^\star(\theta^\star)$. Since $H^\star \succ 0$, $-H^\star$ is Hurwitz and the OU process is exponentially ergodic with stationary law $\mathcal{N}(0, \Sigma_\infty)$. Apply Itô's formula to $\Delta_s\Delta_s^\top$: the drift contributes $-(H^\star\Sigma_s + \Sigma_s H^{\star\top})$ and the quadratic variation contributes $BB^\top$, giving $\frac{d}{ds}\Sigma_s = -H^\star\Sigma_s - \Sigma_s H^{\star\top} + BB^\top$. Setting $\frac{d}{ds}\Sigma_s = 0$ yields (31). Uniqueness follows because for Hurwitz $-H^\star$ the integral $\Sigma_\infty = \int_0^\infty e^{-H^\star s}\,(\tau G^\star)\,e^{-H^{\star\top} s}\,ds$ converges and is the unique solution (Lemma A.4). □

Lyapunov Balance Law (structural consequence of sampling alignment).

The stationary covariance Σ_∞ of the OU regime is determined by three objects: the curvature $H^\star$ (drift), the intrinsic noise geometry $G^\star(\theta^\star)$ (diffusion), and the effective temperature $\tau = \eta/b$ (scale). The Lyapunov equation $H^\star\Sigma_\infty + \Sigma_\infty H^{\star\top} = \tau\,G^\star(\theta^\star)$ is a *structural law*, not a modeling assumption: the diffusion matrix on the right-hand side is not postulated but implied by the mini-batch sampling design (Theorem 4.3). Once the loss and the sampling mechanism are fixed, all three ingredients are determined, and so is the stationary covariance.

Remark 5.9 (Likelihood case (Fisher-aligned diffusion)). If $\ell(\theta; z) = -\log p_\theta(z)$ and the model is correctly specified, then $G^\star(\theta^\star) = F^\star(\theta^\star)$ and the OU diffusion reads

$$d\Delta_s = -H^\star\Delta_s\,ds + \sqrt{\tau}\,C_F^\star\,dW_s, \qquad C_F^\star {C_F^\star}^\top = F^\star(\theta^\star),$$

making Fisher geometry explicit in both transient fluctuations and in the stationary Lyapunov balance (31).

5.4 Fisher-metric coordinates (whitening)

Remark 5.10 (Whitening by the Fisher metric). In Fisher-aligned settings, it is often convenient to work in whitened coordinates $x_s := (F^\star(\theta^\star))^{1/2}\Delta_s$. Formally, the OU drift becomes

$$dx_s = -\Big((F^\star)^{1/2}H^\star(F^\star)^{-1/2}\Big)x_s\,ds + \sqrt{\tau}\,(F^\star)^{1/2}C^\star(\theta^\star)\,dW_s,$$

so contraction is governed by the spectrum of $H^\star$ (equivalently, by the spectrum of the conjugated drift matrix $(F^\star)^{1/2}H^\star(F^\star)^{-1/2}$, which is similar to $H^\star$).

The diffusion limit as an identification tool. The diffusion approximation derived above is not an end in itself. Its role is to *identify* the intrinsic volatility geometry $G^\star(\theta^\star)$ that determines the stationary covariance (Corollary 5.8), the Fisher-risk scaling (Section 6), and the oracle complexity (Section 7). Without the alignment established in Section 4, the diffusion covariance would be a free modeling choice; with it, the covariance is *forced* by the loss and the sampling design, and every downstream quantity inherits this constraint. Two consequences are verified numerically in Section 8: (i) the stationary Fisher-metric risk stabilises at $\mathrm{Tr}(G^\star H^{-1})$, confirming the Lyapunov prediction; and (ii) a trace-matched isotropic surrogate reproduces this scalar but fails to reproduce the off-diagonal covariance structure, confirming that the full geometry—not just the temperature—matters.

6 Convergence Rates in Fisher Geometry

This section establishes *matching* upper and lower bounds for SGD when the error is measured in a *frozen* Fisher metric at a local optimum $\theta^\star$. Once the mini-batch noise covariance is identified (Section 4), the remaining work is a localized stochastic-approximation argument in a fixed geometry, followed by an information-theoretic lower bound expressed in the same metric. *Convention.* All rates in this section are stated in Fisher/Godambe risk $\mathbb{E}[\theta_T^\top F^\star \theta_T]$ unless explicitly noted otherwise; any Euclidean norm that appears is immediately converted.

6.1 Local Fisher Geometry and a Frozen-Metric Regime

Work in a neighborhood of $\theta^\star$ where the Fisher information varies slowly. For clean rate statements we freeze the metric

$$F^\star := F(\theta^\star), \qquad \|v\|_{F^\star}^2 := v^\top F^\star v.$$

(Allowing a slowly varying metric $F(\theta)$ is standard via localization; the frozen-metric bounds below are the local core and are what we use later for oracle complexity.)

Lemma 6.1 (Sufficient condition for the frozen-metric regime)**.** *Suppose $F(\theta)$ is Lipschitz on a neighborhood $\mathcal{U}$ of $\theta^\star$: $\|F(\theta) - F(\theta^\star)\|_{\mathrm{op}} \le L_F \|\theta - \theta^\star\|_2$ for all $\theta \in \mathcal{U}$. If the SGD iterates satisfy $\|\theta_t - \theta^\star\|_2 = o(1)$ almost surely, then for every $\epsilon > 0$ there exists t_0 such that for $t \ge t_0$, $(1-\epsilon)F^\star \preceq F(\theta_t) \preceq (1+\epsilon)F^\star$. In particular, the frozen-metric approximation $\|\cdot\|_{F^\star}$ and $\|\cdot\|_{F(\theta_t)}$ are equivalent up to multiplicative $(1 \pm \epsilon)$ for all sufficiently late iterates.*

Let $h(\theta) := \nabla L(\theta)$ and decompose the mini-batch estimator as

$$g_t(\theta_t) = h(\theta_t) + \xi_t, \qquad \mathbb{E}[\xi_t \mid \mathcal{F}_t] = 0,$$

where $\mathcal{F}_t$ is the natural filtration. Under Fisher alignment (Section 4), the conditional covariance

satisfies the local approximation

$$\mathbb{E}[\xi_t \xi_t^\top \mid \mathcal{F}_t] \;=\; \frac{1}{b} F^\star \;+\; r_t, \qquad \|r_t\|_{\mathrm{op}} \le \frac{c_r}{b}\, \rho_t, \tag{33}$$

with $\rho_t \to 0$ in the local regime.

Define the Fisher-strong-convexity constant at $\theta^\star$:

$$\mu_F \;:=\; \lambda_{\min}\left(\frac{(F^\star)^{1/2} H^\star (F^\star)^{-1/2} + (F^\star)^{-1/2} H^\star (F^\star)^{1/2}}{2} \right), \qquad H^\star := \nabla^2 L(\theta^\star). \tag{34}$$

Define the effective dimension

$$d_{\mathrm{eff}}(F^\star) \;:=\; \frac{\mathrm{Tr}(F^\star)}{\|F^\star\|_{\mathrm{op}}} \;=\; \frac{\mathrm{Tr}(F^\star)}{\lambda_{\max}(F^\star)} \;\in (0, d]. \tag{35}$$

Remark 6.2 (Effective dimension as stable rank). The quantity $d_{\mathrm{eff}}(F^\star)$ is exactly the *stable rank* of $F^\star$, a standard measure of intrinsic dimensionality that is robust to small perturbations (Tropp, 2015). Three properties make d_{eff} the appropriate dimensional parameter for Fisher-metric rates: (i) $d_{\mathrm{eff}} \le d$ always, with equality if and only if all eigenvalues of $F^\star$ coincide (isotropic Fisher geometry); (ii) d_{eff} can be much smaller than d when Fisher information is concentrated in a few directions—the extreme case $d_{\mathrm{eff}} \to 1$ occurs when a single direction dominates; (iii) d_{eff} replaces the ambient dimension d in both the upper bound (Theorem 6.4) and the oracle complexity (Theorem 7.3). The distinction is operationally significant: classical Euclidean bounds scale with the ambient dimension d, whereas the Fisher-metric bounds scale with d_{eff}, reflecting only the statistically distinguishable directions. In problems where information is concentrated (e.g., sparse or low-rank Fisher structure), $d_{\mathrm{eff}} \ll d$ and the Fisher-metric guarantee is correspondingly tighter.

6.2 Upper Bound

Lemma 6.3 (One-step Fisher Lyapunov drift)**.** *Let $\Delta_t := \theta_t - \theta^\star$ and $V_t := \|\Delta_t\|_{F^\star}^2$. Assume: (i) L is locally M-smooth near $\theta^\star$; (ii) $H^\star \succ 0$; (iii) (33) holds. Then, as long as θ_t stays in the local neighborhood,*

$$\mathbb{E}[V_{t+1} \mid \mathcal{F}_t] \;\le\; \Big(1 - 2\mu_F \eta_t + c_0 \eta_t^2\Big) V_t \;+\; \eta_t^2 \frac{1}{b} \mathrm{Tr}\big((F^\star)^2\big) \;+\; \eta_t^2 \frac{c_1}{b} \mathrm{Tr}(F^\star)\, \rho_t, \tag{36}$$

where c_0, c_1 depend only on $(M, \|F^\star\|_{\mathrm{op}}, c_r)$.

Proof. From $\theta_{t+1} = \theta_t - \eta_t(h(\theta_t) + \xi_t)$, $\Delta_{t+1} = \Delta_t - \eta_t h(\theta_t) - \eta_t \xi_t$. Expanding $V_{t+1} = \Delta_{t+1}^\top F^\star \Delta_{t+1}$ and taking conditional expectation (using $\mathbb{E}[\xi_t \mid \mathcal{F}_t] = 0$) yields

$$\mathbb{E}[V_{t+1} \mid \mathcal{F}_t] = V_t - 2\eta_t \Delta_t^\top F^\star h(\theta_t) + \eta_t^2\, h(\theta_t)^\top F^\star h(\theta_t) + \eta_t^2\, \mathrm{Tr}\Big(F^\star\, \mathbb{E}[\xi_t \xi_t^\top \mid \mathcal{F}_t]\Big).$$

Using $h(\theta^\star + \Delta) = H^\star\Delta + o(\|\Delta\|)$, we have $\Delta_t^\top F^\star h(\theta_t) = \Delta_t^\top F^\star H^\star \Delta_t + o(V_t)$. Writing $x_t := (F^\star)^{1/2}\Delta_t$ gives $\Delta_t^\top F^\star H^\star \Delta_t = x_t^\top \operatorname{Sym}\big((F^\star)^{1/2} H^\star (F^\star)^{-1/2}\big)\, x_t \geq \mu_F V_t$. Local M-smoothness implies $h(\theta_t)^\top F^\star h(\theta_t) \leq c_0 V_t$. For the noise term, plug (33):

$$\operatorname{Tr}\Big(F^\star\, \mathbb{E}[\xi_t \xi_t^\top \mid \mathcal{F}_t]\Big) = \frac{1}{b}\operatorname{Tr}((F^\star)^2) + \operatorname{Tr}(F^\star r_t).$$

Finally $|\operatorname{Tr}(F^\star r_t)| \lesssim \operatorname{Tr}(F^\star)\|r_t\|_{\mathrm{op}} \leq (c_1/b)\operatorname{Tr}(F^\star)\rho_t$, giving (36). □

Theorem 6.4 (Upper bound in frozen Fisher geometry)**.** *Assume Lemma 6.3. Take $\eta_t = \eta_0/t$ with $\eta_0 > 1/(2\mu_F)$, and assume $\sum_{t\geq 1}\eta_t^2\rho_t < \infty$. Then for all $T \geq 2$,*

$$\mathbb{E}\Big[\|\theta_T - \theta^\star\|_{F^\star}^2\Big] \;\leq\; \frac{C_1}{b}\cdot\frac{\operatorname{Tr}((F^\star)^2)}{\mu_F}\cdot\frac{1}{T} \;+\; C_2\cdot\frac{\|\theta_1-\theta^\star\|_{F^\star}^2}{T^{2\mu_F\eta_0}} \;+\; \frac{C_3}{b}\cdot\frac{\operatorname{Tr}(F^\star)}{T}, \tag{37}$$

where C_1, C_2, C_3 depend only on $(\eta_0, \mu_F, c_0, c_1)$.

Moreover, using $\operatorname{Tr}((F^\star)^2) \leq \lambda_{\max}(F^\star)\operatorname{Tr}(F^\star)$, we obtain

$$\begin{aligned}\mathbb{E}\Big[\|\theta_T - \theta^\star\|_{F^\star}^2\Big] \;&\leq\; \frac{\widetilde{C}_1}{b}\cdot\frac{\lambda_{\max}(F^\star)\operatorname{Tr}(F^\star)}{\mu_F}\cdot\frac{1}{T} \;+\; \widetilde{C}_2\cdot\frac{\|\theta_1-\theta^\star\|_{F^\star}^2}{T^{2\mu_F\eta_0}}\\ &=\; \frac{\widetilde{C}_1}{b}\cdot\frac{\lambda_{\max}(F^\star)^2}{\mu_F}\cdot\frac{d_{\mathrm{eff}}(F^\star)}{T} \;+\; \widetilde{C}_2\cdot\frac{\|\theta_1-\theta^\star\|_{F^\star}^2}{T^{2\mu_F\eta_0}}.\end{aligned} \tag{38}$$

Proof. Take total expectations in (36) to obtain $\mathbb{E}[V_{t+1}] \leq a_t\,\mathbb{E}[V_t] + u_t$ with $a_t := 1 - 2\mu_F\eta_t + c_0\eta_t^2$ and $u_t := \eta_t^2\frac{1}{b}\operatorname{Tr}((F^\star)^2) + \eta_t^2\frac{c_1}{b}\operatorname{Tr}(F^\star)\rho_t$. For $\eta_t = \eta_0/t$, there exists t_0 such that for $t \geq t_0$, $a_t \leq 1 - \mu_F\eta_0/t$. Define $A_{t,T} := \prod_{s=t}^{T-1} a_s$. Unrolling gives $\mathbb{E}[V_T] \leq A_{1,T}V_1 + \sum_{t=1}^{T-1} A_{t+1,T}u_t$. Standard product bounds yield $A_{1,T} \leq CT^{-2\mu_F\eta_0}$ and $A_{t+1,T} \leq C(t/T)^{\mu_F\eta_0}$. Then, since $\mu_F\eta_0 > 1/2$, $\sum_{t\leq T} A_{t+1,T}\eta_t^2 = O(1/T)$, giving the leading $(\operatorname{Tr}((F^\star)^2)/b)(1/T)$ term. The remainder term is controlled because $\sum_t \eta_t^2\rho_t < \infty$ and $A_{t+1,T} \leq 1$, yielding an additional $O((\operatorname{Tr}(F^\star)/b)(1/T))$ contribution. This proves (37). The reduction to (38) follows from $\operatorname{Tr}((F^\star)^2) \leq \lambda_{\max}(F^\star)\operatorname{Tr}(F^\star)$. □

Remark 6.5 (OU viewpoint and the same $1/T$ scaling)*.* In the local regime, the diffusion limit yields a (time-rescaled) OU approximation whose diffusion coefficient is proportional to the frozen mini-batch covariance $F^\star/b$. With a diminishing schedule $\eta_t \asymp 1/t$, this perspective is consistent with the discrete-time bound: the mean-square error in the frozen Fisher norm decays on the order of $1/(Tb)$, with constants governed by $F^\star$ and the intrinsic curvature μ_F.

6.3 Lower Bound

Assumption 6.6 (Oracle–information structure)**.** The oracle produces observations $Y_t = \psi(\theta_t; Z_t)$, where:

(i) θ_t is $\mathcal{F}_{t-1}$-measurable, with filtration $\mathcal{F}_t := \sigma(Y_1, \ldots, Y_t)$;

(ii) *Conditional unbiasedness:* $\mathbb{E}_{\theta^\star}[Y_t \mid \mathcal{F}_{t-1}] = 0$;

(iii) *Predictable information bound:* $\mathbb{E}_{\theta^\star}[Y_t Y_t^\top \mid \mathcal{F}_{t-1}] \preceq \mathcal{I}_1(\theta^\star)$, a.s., where $\mathcal{I}_1(\theta^\star) := F(\theta^\star) = F^\star$ in the likelihood case;

(iv) *Uniform moment control:* $\sup_t \mathbb{E}_{\theta^\star}\|Y_t\|^4 < \infty$.

The oracle transcript $(\theta_0, Y_1, \ldots, Y_N)$ thus forms a martingale difference sequence with predictable quadratic variation bounded by $\mathcal{I}_1$.

Remark 6.7 (Beyond i.i.d. oracles). The classical setting of i.i.d. sampling from $P_{\theta^\star}$ satisfies Assumption 6.6 with equality in (iii). However, the lower bound argument does not fundamentally rely on independence across oracle calls. What is required is a *predictable quadratic-variation bound* on the oracle transcript. This accommodates exchangeable or conditionally i.i.d. sampling schemes (e.g., de Finetti mixtures) provided the cumulative information growth is bounded by $N\mathcal{I}_1$. In this sense, the lower bound below is not a direct transposition of the classical i.i.d. van Trees proof but an oracle-information statement tailored to stochastic optimization.

Theorem 6.8 (Minimax lower bound in Fisher metric)**.** *Suppose Assumption 6.6 holds and $F^\star := F(\theta^\star) \succ 0$. Let the parametric family $\{P_\theta : \theta \in \Theta_{\mathrm{loc}}\}$ satisfy the regularity conditions of the van Trees inequality on a neighborhood Θ_{loc} of $\theta^\star$ (see Gill and Levit (1995); the connection to local asymptotic normality and intrinsic statistical distance is developed in Le Cam (1986); the key requirements are smoothness and integrability of the Fisher information on Θ_{loc}). Then*

$$\inf_{\hat{\theta}_N} \sup_{\theta \in \Theta_{\mathrm{loc}}} \mathbb{E}_\theta\Big[\|\hat{\theta}_N - \theta\|^2_{F(\theta)}\Big] \;\geq\; \frac{c\,d}{N}, \tag{39}$$

for a universal constant $c > 0$.

In particular, if one SGD iteration uses a mini-batch of size b (so $N = Tb$ oracle calls), then $\inf_{\hat{\theta}_T} \sup_\theta \mathbb{E}[\|\hat{\theta}_T - \theta\|^2_{F(\theta)}] \geq c\,d/(Tb)$.

Proof. **Step 1 (predictable information accumulation).** By Assumption 6.6(iii), the predictable quadratic variation of the oracle transcript satisfies

$$\sum_{t=1}^{N} \mathbb{E}_{\theta^\star}\big[Y_t Y_t^\top \mid \mathcal{F}_{t-1}\big] \;\preceq\; N\,\mathcal{I}_1(\theta^\star).$$

Thus the total predictable information in the oracle transcript is bounded by $N\mathcal{I}_1(\theta^\star)$.

Step 2 (transcript measurability). Since the estimator $\hat{\theta}_N$ is $\mathcal{F}_N$-measurable, its Fisher information cannot exceed the predictable information accumulated in the oracle transcript.

Step 3 (van Trees inequality). Apply the van Trees inequality with a smooth prior π supported on Θ_{loc}: $\mathbb{E}_\pi\mathbb{E}[(\hat{\theta}-\theta)(\hat{\theta}-\theta)^\top] \succeq (N\mathcal{I}_1 + J_\pi)^{-1}$. Multiply by $F^\star$ and take traces: $\mathbb{E}_\pi\mathbb{E}[\|\hat{\theta}-\theta\|_{F^\star}^2] \geq \operatorname{Tr}(F^\star(N\mathcal{I}_1+J_\pi)^{-1})$. In the likelihood case, $\mathcal{I}_1 = F^\star$, so choose π with $J_\pi \preceq c_0 F^\star$ on Θ_{loc}, yielding $\operatorname{Tr}(F^\star(NF^\star + J_\pi)^{-1}) \geq \operatorname{Tr}(I_d)/(N+c_0) \geq c\,d/N$ for a universal $c > 0$. □

Corollary 6.9 (i.i.d. oracle)**.** *If the oracle draws are i.i.d. $\sim P_{\theta^\star}$, then Assumption 6.6 holds with equality in (iii) and $\mathcal{I}_1(\theta^\star) = F^\star$. The lower bound (39) reduces to the classical Fisher-information scaling $\Omega(d/N)$.*

Corollary 6.10 (Matching rates (up to constants))**.** *Under Theorem 6.4 and the oracle model of Assumption 6.6,*

$$\mathbb{E}\Big[\|\theta_T - \theta^\star\|_{F^\star}^2\Big] = \Theta\Big(\frac{1}{Tb}\Big) \quad \textit{equivalently} \quad \Theta\Big(\frac{1}{N}\Big) \textit{ per oracle call}, \quad N = Tb.$$

7 Oracle Complexity

This section turns the Fisher-geometry mean-square bounds of Section 6 into an explicit *oracle-complexity* guarantee for achieving ε-stationarity. The steps are standard—smoothness descent, averaged-gradient bound, martingale concentration (cf. Nesterov, 2004, Chapter 2)—but we express the result in the natural Fisher dual norm and keep the statistical conditioning explicit.

Throughout, we work locally near $\theta^\star$ and freeze the metric $F^\star := F(\theta^\star) \succ 0$ (for general losses, replace $F^\star$ by $G^\star(\theta^\star)$; see Remark 7.5).

7.1 Stationarity in the Fisher dual norm

Definition 7.1 (ε-stationarity in Fisher dual norm)**.** Let $F^\star \succ 0$. We say θ is *ε-stationary* (in the Fisher metric) if

$$\|\nabla L(\theta)\|_{(F^\star)^{-1}} \;:=\; \sqrt{\nabla L(\theta)^\top (F^\star)^{-1} \nabla L(\theta)} \;\leq\; \varepsilon.$$

7.2 From Fisher distance to Fisher-dual stationarity

Lemma 7.2 (Distance-to-stationarity conversion)**.** *Assume L is M-smooth on a neighborhood $\mathcal{U}$ of $\theta^\star$ and $F^\star \succ 0$. Then for all $\theta \in \mathcal{U}$,*

$$\|\nabla L(\theta)\|_{(F^\star)^{-1}}^2 \;\leq\; \frac{M^2}{\lambda_{\min}(F^\star)^2}\,\|\theta-\theta^\star\|_{F^\star}^2. \tag{40}$$

Moreover, if $\theta \to \theta^\star$ and $\nabla L(\theta) = H^\star(\theta-\theta^\star) + o(\|\theta-\theta^\star\|)$, then locally

$$\|\nabla L(\theta)\|_{(F^\star)^{-1}}^2 \;\leq\; (1+o(1))\,\lambda_{\max}\big(F^{\star -1/2} H^\star F^{\star -1/2}\big)^2\,\|\theta-\theta^\star\|_{F^\star}^2. \tag{41}$$

Proof. By M-smoothness and $\nabla L(\theta^\star) = 0$, $\|\nabla L(\theta)\|_2 \le M\|\theta - \theta^\star\|_2$. The dual-norm bound $\|v\|^2_{(F^\star)^{-1}} \le \lambda_{\min}(F^\star)^{-1}\|v\|_2^2$ converts Euclidean gradient norm to Fisher dual norm, and $\|\theta - \theta^\star\|_2^2 \le \lambda_{\min}(F^\star)^{-1}\|\theta - \theta^\star\|^2_{F^\star}$ converts Fisher distance to Euclidean. Combining: $\|\nabla L\|^2_{(F^\star)^{-1}} \le \lambda_{\min}(F^\star)^{-1} M^2 \lambda_{\min}(F^\star)^{-1}\|\theta - \theta^\star\|^2_{F^\star} = M^2/\lambda_{\min}(F^\star)^2 \cdot \|\theta - \theta^\star\|^2_{F^\star}$. The local refinement follows by replacing M by $\|H^\star\|_{\mathrm{op}}$ up to $1 + o(1)$ via the linearization. □

7.3 High-probability oracle complexity

Theorem 7.3 (Oracle complexity for Fisher-dual stationarity)**.** *Assume the local regularity conditions of Section 3 hold on a neighborhood $\mathcal{U}$ of $\theta^\star$, and suppose that on $\mathcal{U}$ the mini-batch noise is Fisher-aligned in the sense that, for some batch size $b \ge 1$,*

$$\mathbb{E}[\xi_t \mid \mathcal{F}_t] = 0, \qquad \mathbb{E}[\xi_t \xi_t^\top \mid \mathcal{F}_t] \preceq \frac{1}{b} F^\star. \tag{42}$$

Run SGD with constant batch size b and constant stepsize $\eta \le 1/(4M)$:

$$\theta_{t+1} = \theta_t - \eta\big(\nabla L(\theta_t) + \xi_t\big).$$

Define the Fisher condition number and intrinsic dimension

$$\kappa_F := \frac{\lambda_{\max}(F^\star)}{\lambda_{\min}(F^\star)}, \qquad d_{\mathrm{eff}}(F^\star) := \frac{\mathrm{Tr}(F^\star)}{\lambda_{\max}(F^\star)}.$$

Then there exists a universal constant $C > 0$ such that, for any $\delta \in (0,1)$, with probability at least $1 - \delta$,

$$\min_{0 \le t \le T-1} \|\nabla L(\theta_t)\|^2_{(F^\star)^{-1}} \;\le\; C\left(\frac{L(\theta_0) - L(\theta^\star)}{\eta\, T\, \lambda_{\min}(F^\star)} \;+\; \frac{\eta}{b}\,\kappa_F\, d_{\mathrm{eff}}(F^\star)\right)\log\frac{1}{\delta}. \tag{43}$$

In particular, choosing (η, T) so that the right-hand side is $\le \varepsilon^2$ implies $\min_{t<T} \|\nabla L(\theta_t)\|_{(F^\star)^{-1}} \le \varepsilon$ with probability at least $1 - \delta$.

Equivalently, in terms of oracle calls $N := Tb$ *(sample-gradient evaluations), one sufficient scaling (up to constants and ignoring the transient term $\frac{L(\theta_0) - L(\theta^\star)}{\eta T \lambda_{\min}(F^\star)}$) is*

$$N \;=\; \Theta\!\left(\frac{\kappa_F\, d_{\mathrm{eff}}(F^\star)}{\varepsilon^2}\,\log\frac{1}{\delta}\right). \tag{44}$$

Proof. **Step 1 (descent inequality).** By M-smoothness and $\eta \le 1/(4M)$, expand $L(\theta_{t+1}) \le L(\theta_t) + \langle \nabla L, \theta_{t+1} - \theta_t\rangle + \frac{M}{2}\|\theta_{t+1} - \theta_t\|^2$ with $\theta_{t+1} - \theta_t = -\eta(\nabla L(\theta_t) + \xi_t)$. After expanding and using $\eta \le 1/(4M)$, so $1 - M\eta/2 \ge 1 - 1/8 = 7/8$ and $\eta M \le 1/4$:

$$L(\theta_{t+1}) \le L(\theta_t) - \tfrac{3\eta}{4}\|\nabla L(\theta_t)\|_2^2 + \eta(1 + M\eta)\langle \nabla L(\theta_t), \xi_t\rangle + \tfrac{M\eta^2}{2}\|\xi_t\|_2^2.$$

Step 2 (define martingale). Let $\Delta M_{t+1} := \eta\langle \nabla L(\theta_t), \xi_t\rangle$ and $M_T := \sum_{t=0}^{T-1} \Delta M_{t+1}$; since $\mathbb{E}[\xi_t \mid \mathcal{F}_t] = 0$, this is a martingale.

Step 3 (sum the descent). Summing from $t = 0$ to $T-1$ and using $\mathbb{E}[\|\xi_t\|_2^2 \mid \mathcal{F}_t] \le b^{-1}\mathrm{Tr}(F^\star)$:

$$\tfrac{3\eta}{4}\sum_{t=0}^{T-1} \|\nabla L(\theta_t)\|_2^2 \;\le\; \Delta L + C_1 M_T + \tfrac{M\eta^2 T}{2b}\,\mathrm{Tr}(F^\star), \quad \Delta L := L(\theta_0) - L(\theta^\star).$$

Step 4 (apply Freedman's inequality). The predictable quadratic variation satisfies $\langle M\rangle_T \le (\eta^2/b)\mathrm{Tr}(F^\star)\sum_{t<T}\|\nabla L(\theta_t)\|_2^2$. The increments $\Delta M_{t+1} = \eta\langle \nabla L(\theta_t), \xi_t\rangle$ have bounded conditional variance $\mathbb{E}[(\Delta M_{t+1})^2 \mid \mathcal{F}_t] \le \eta^2\|\nabla L(\theta_t)\|_2^2 \cdot b^{-1}\mathrm{Tr}(F^\star)$, and satisfy $|\Delta M_{t+1}| \le R$ almost surely for $R := \eta\, M\, \mathrm{diam}(\mathcal{U}) \cdot b^{-1/2}\|F^\star\|_{\mathrm{op}}^{1/2}$ (using Cauchy–Schwarz and the bounded-gradient condition on $\mathcal{U}$). By Freedman's inequality (Lemma A.7), with probability at least $1-\delta$, $M_T \le c\sqrt{\langle M\rangle_T \log(1/\delta)} + c' R \log(1/\delta)$.

Step 5 (solve for gradient bound). Let $S_T := \sum_{t<T}\|\nabla L(\theta_t)\|_2^2$. Substituting into Step 3 gives a quadratic inequality in $\sqrt{S_T}$; solving:

$$\min_{t<T}\|\nabla L(\theta_t)\|_2^2 \;\le\; \frac{S_T}{T} \;\le\; C\Big(\frac{\Delta L}{\eta T} + \frac{\eta}{b}\mathrm{Tr}(F^\star)\Big)\log\frac{1}{\delta}.$$

Step 6 (Fisher dual norm). Use $\|v\|_{(F^\star)^{-1}}^2 \le \lambda_{\min}(F^\star)^{-1}\|v\|_2^2$ and $\mathrm{Tr}(F^\star)/\lambda_{\min}(F^\star) = \kappa_F\, d_{\mathrm{eff}}(F^\star)$:

$$\min_{t<T}\|\nabla L(\theta_t)\|_{(F^\star)^{-1}}^2 \;\le\; C\Big(\frac{\Delta L}{\eta T\lambda_{\min}(F^\star)} + \frac{\eta}{b}\,\kappa_F\, d_{\mathrm{eff}}(F^\star)\Big)\log\frac{1}{\delta},$$

establishing (43). The oracle complexity (44) follows by balancing the two terms and setting $N = Tb$. □

Remark 7.4 (Statistical vs. Euclidean conditioning). Classical oracle-complexity results for first-order methods express the iteration count through the Euclidean (Hessian) condition number $\kappa_H := \lambda_{\max}(H^\star)/\lambda_{\min}(H^\star)$ and the ambient dimension d. In (44), these quantities are replaced by their statistical counterparts: the Fisher condition number $\kappa_F = \lambda_{\max}(F^\star)/\lambda_{\min}(F^\star)$ and the effective dimension $d_{\mathrm{eff}}(F^\star)$. The substitution is not cosmetic. A problem may be Euclidean-stiff ($\kappa_H \gg 1$) yet statistically well-conditioned ($\kappa_F = O(1)$) when curvature and Fisher information share the same eigenstructure, so that difficult curvature directions coincide with informative ones. Conversely, isotropic curvature ($\kappa_H = 1$) does not guarantee favorable statistical complexity if information is anisotropic. The replacement of (κ_H, d) by $(\kappa_F, d_{\mathrm{eff}})$ reflects the fact that, once noise geometry is identified, the fundamental bottleneck in stochastic optimization is statistical resolution, not algebraic curvature.

Remark 7.5 (General losses / Godambe geometry). For general losses, replace $F^\star$ by $G^\star(\theta^\star)$ throughout and interpret the dual norm accordingly. The alignment condition (42) is then exactly the local conclusion of Theorem 4.3.

Remark 7.6 (Iteration vs. oracle complexity). Equation (44) counts *oracle calls* $N = Tb$. If reporting iteration complexity, keep b explicit and interpret $T = N/b$.

Remark 7.7 (Interpreting the complexity constants). The oracle complexity (44) is governed by two geometry-dependent quantities:

- $\kappa_F = \lambda_{\max}(F^\star)/\lambda_{\min}(F^\star)$ is the *Fisher condition number*—the ratio of maximal to minimal statistical information per coordinate direction. Large κ_F signals that some parameter directions are much harder to resolve than others.
- $d_{\text{eff}}(F^\star) = \text{Tr}(F^\star)/\lambda_{\max}(F^\star)$ is the *effective dimension* (stable rank of $F^\star$): the number of statistically distinguishable directions under the curvature-weighted geometry (see Remark 6.2).

The product $\kappa_F\, d_{\text{eff}}$ thus measures the total cost of resolving all statistically relevant directions at the hardest direction's scale. Importantly, (44) is not merely a rate statement: it is a *design law* that links the practitioner's sampling budget N to achievable stationarity through intrinsic problem geometry. All modeling freedom has been eliminated—once the loss and sampling design are fixed, the complexity is determined.

Corollary 7.8 (Batch-size scaling under a fixed sample budget)**.** *Fix a total sampling budget N and run $T = N/b$ iterations of constant-stepsize SGD with batch size b. Equating the bias term $\sim (L(\theta_0) - L^\star)/(\eta T \lambda_{\min}(F^\star))$ and the variance term $\sim \eta \kappa_F d_{\text{eff}}/b$ in (43) yields the balanced stepsize $\eta^\star \propto \sqrt{b/(T\kappa_F d_{\text{eff}})}$. Substituting $T = N/b$, the resulting Fisher-dual stationarity gap satisfies*

$$\min_{t<T} \|\nabla L(\theta_t)\|^2_{(F^\star)^{-1}} \;=\; \mathcal{O}\left(\sqrt{\frac{\kappa_F\, d_{\text{eff}}}{N}}\right),$$

which is independent of b at leading order. The practical implication for OR settings is that, under this budget-constrained regime, small batches lose nothing in worst-case guarantee while gaining more frequent iterates; the Fisher/Godambe geometry determines the constant *but not the* scaling *in N.*

8 Numerical Validation

The numerical experiments are small and diagnostic by design. Each is chosen so that (i) a clean theoretical benchmark is available (Lyapunov/OU or discrete Lyapunov), and (ii) the benchmark isolates exactly the mechanism emphasized by the theory: Fisher/Godambe-aligned diffusion, anisotropy, and propagation under curvature. Rather than reporting large tables of means and standard errors, we let the figures carry the evidence; the data-generating scripts record all replicate-level outputs for reproducibility.

Table 2: Reproducibility capsule: key experimental parameters.

Experiment	d	Replicates	η	Steps	Sweep variable
1 (Batch scaling)	2	500	0.05	200 000	$b \in \{1, 2, 4, \ldots, 512\}$
2 (Angle sweep)	2	500	0.05	200 000	$\theta \in [0, \pi/2]$
3 (Rotation smoking gun)	2	—	—	—	$\phi \in [0, \pi/2]$ (theory)
4 (OU plateau, $d{=}10$)	10	2 000	$0.5/\lambda_{\max}$	300–10 000	T (horizon)
5 ($1/N$ rate)	10	800	$\eta_0/(t{+}t_0)$	600–9 600	$N = Tb$
6 (Directional var.)	10	800	$\eta_0/(t{+}t_0)$	600–9 600	eigenvectors of $G^\star$

Experiments 1–3: Euler–Maruyama, $d = 2$. Experiments 4–6: direct SGD recursion, $d = 10$, $b = 64$.

Reproducibility. Table 2 summarizes the experimental parameters. All experiments use $d = 2$, Euler–Maruyama discretization, and $R = 500$ independent replicates per configuration. Code is available in the supplementary material.

The experiments are organized around three claims. Each claim is followed by experiments that validate it and a "so what" connecting it to an OR design implication.

8.1 Claim 1: The Lyapunov Equilibrium Law Is Quantitatively Predictive

The first claim is that the Fisher–Lyapunov balance (Corollary 5.8) is not merely a qualitative insight but a quantitatively accurate prediction of steady-state risk, and that the *shape* of the noise covariance—not just its scale—governs which directions receive noise energy at equilibrium. Three experiments validate this at increasing dimensionality.

8.1.1 Experiment 1: Fisher–Lyapunov Equilibrium and $1/b$ Scaling (OU Benchmark).

Setup. We begin with the local OU surrogate implied by the diffusion limit near a nondegenerate optimum:

$$d\theta_t \;=\; -\eta\, H\, \theta_t\, dt \;+\; \sqrt{\frac{2\eta}{b}}\; F^{1/2}\, dW_t, \tag{45}$$

where $H \succ 0$ is the local curvature, $F \succeq 0$ is the Fisher/Godambe noise shape, η is a stepsize scale, and b is the batch size. We choose a two-dimensional sharp/flat curvature $H = \mathrm{diag}(1, 0.1)$ and take $F = I_2$, then sweep b over a wide range.

Benchmark. At stationarity, the covariance $\Sigma(b)$ solves the Lyapunov equation

$$H\Sigma + \Sigma H \;=\; \frac{2}{b}\, F, \tag{46}$$

so every stationary marginal variance scales as $1/b$. Importantly, η does not appear in the equilibrium covariance; it governs mixing time, not the fixed point.

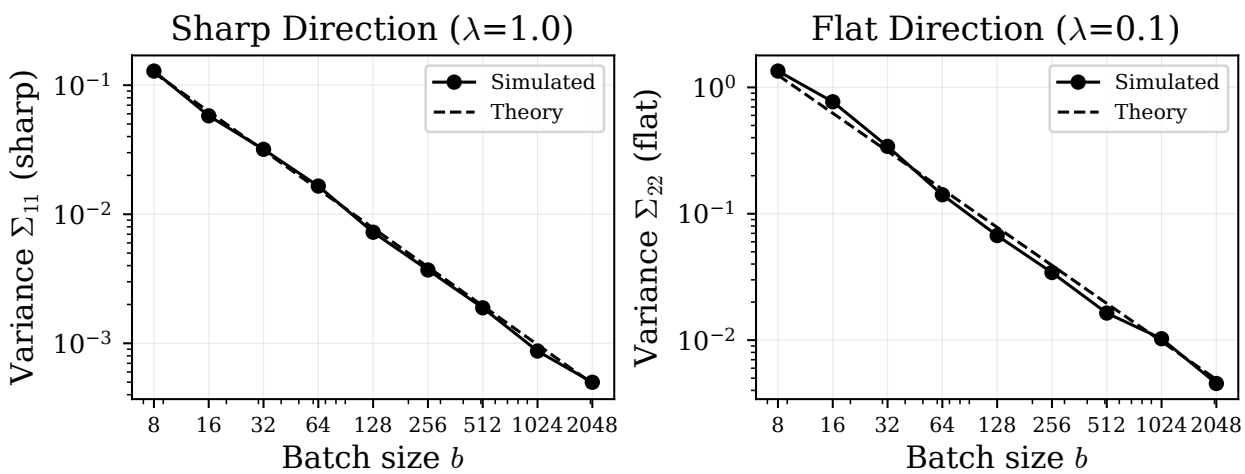

Figure 2: OU benchmark: stationary variances vs. batch size b (log scales). Solid: simulation; dashed: Lyapunov prediction from (46).

$d = 2$, $H = \mathrm{diag}(1, 0.1)$, $F = I_2$, 500 replicates per batch size, 200 000 steps each.

What the figure shows. Figure 2 overlays simulated stationary variances with the Lyapunov prediction and shows clean $1/b$ scaling across the batch sweep. The flat coordinate mixes more slowly (as expected under weak curvature) but converges to the same equilibrium law. This serves as a baseline sanity check: the Fisher–Lyapunov equilibrium is not merely qualitative; it is quantitatively predictive. We observed early entry into the basin of Fisher geometry even from random starts; see Section 9.3 for a diagnostic based on the stability ratios δ_F and δ_H.

8.1.2 Experiment 2: Anisotropic Fisher–Hessian Misalignment (Angle Sweep).

Setup. We keep the same sharp/flat curvature $H = \mathrm{diag}(1, 0.1)$, but rotate an anisotropic noise-shape matrix relative to the curvature basis:

$$F(\varphi) = R(\varphi) \begin{pmatrix} 1.5 & 0 \\ 0 & 0.5 \end{pmatrix} R(\varphi)^\top, \qquad \varphi \in [0, \pi/3],$$

with fixed batch size. This experiment isolates *alignment* as an operational parameter: the eigenvectors of F move while H is held fixed.

Benchmark. Because the simulator is Euler–Maruyama with finite time step, the appropriate theoretical comparator is the *discrete* Lyapunov equation induced by the one-step dynamics. Writing $A = I - \eta H \Delta t$ and $Q = (2\eta/b)F(\theta)\Delta t$, the stationary covariance solves

$$\Sigma \;=\; A\Sigma A^\top + Q. \tag{47}$$

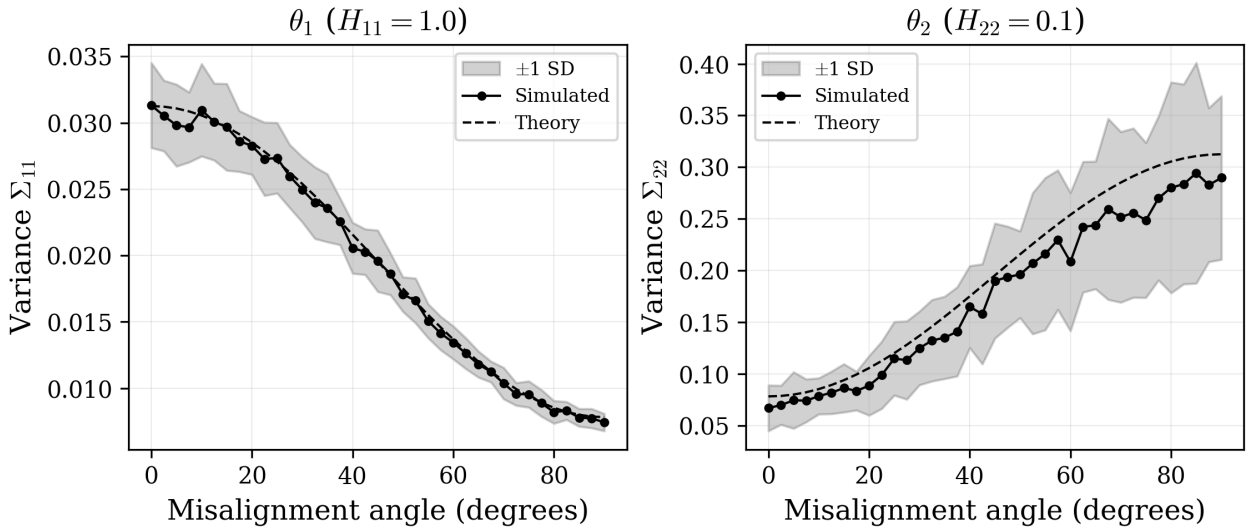

Figure 3: Angle sweep: stationary variances vs. misalignment angle. Bands show replicate variability; dashed curves are the discrete Lyapunov prediction from (47).

$d = 2$, $H = \mathrm{diag}(1, 0.1)$, anisotropic $F(\theta)$ rotated over $[0, \pi/2]$, 500 replicates per angle.

This removes discretization ambiguity and provides a clean, implementable target.

What the figure shows. Figure 3 shows a clear transfer of stationary variance across coordinates as θ varies: when the noise eigenbasis rotates away from the curvature eigenbasis, equilibrium variance is redistributed in a predictable way. The discrete Lyapunov benchmark tracks the simulation closely across the sweep. The takeaway is structural: *alignment governs which directions receive noise energy at equilibrium*, even when scalar temperature η/b is held fixed.

8.1.3 Experiment 4: OU/Lyapunov Plateau in $d = 10$ (Anisotropic vs. Isotropic).

Experiments 1–2 used $d = 2$. We now move to $d = 10$ to validate the Lyapunov equilibrium in a setting where anisotropy is richer. The curvature is $H = \mathrm{diag}(\lambda_1, \ldots, \lambda_{10})$ with eigenvalues log-spaced between 1 and 100. The noise shape $G^\star$ is a random SPD matrix with eigenvalues log-spaced between 0.5 and 5; we also compare an isotropic control $G_{\mathrm{iso}} = \sigma^2 I$ with $\sigma^2 = \mathrm{Tr}(G^\star)/d$ (trace-matched).

Setup. Under constant step size $\eta = 0.5/\lambda_{\max}(H)$ and batch size $b = 64$, we run $R = 2{,}000$ replicates and record the Fisher-metric risk $\mathbb{E}[\|\theta_T\|^2_{F^\star}]$ over increasing horizons $T \in \{300, 800, 2000, 5000, 10000\}$.

What the table shows. Table 3 confirms the Lyapunov prediction (Corollary 5.8): both the anisotropic and isotropic empirical risks converge to the predicted stationary level as T grows. The convergence ratio $\widehat{R}/R_\infty$ approaches unity from both sides, confirming that the discrete Lyapunov

	Empirical Risk $\widehat{R}_T$		Lyapunov R_∞		$\widehat{R}_T/R_\infty$	
T	Aniso	Iso	Aniso	Iso	Aniso	Iso
300	8.55×10^{-4}	8.60×10^{-4}	8.63×10^{-4}	8.58×10^{-4}	0.991	1.002
800	8.64×10^{-4}	8.49×10^{-4}			1.002	0.990
2 000	8.58×10^{-4}	8.50×10^{-4}			0.995	0.992
5 000	8.72×10^{-4}	8.58×10^{-4}			1.010	1.001
10 000	8.63×10^{-4}	8.47×10^{-4}			1.000	0.987

Table 3: OU/Lyapunov plateau ($d = 10$): empirical Fisher-metric risk vs. discrete Lyapunov prediction $R_\infty = \mathrm{Tr}(F^\star\Sigma_\infty)$. Convergence ratios $\widehat{R}_T/R_\infty \to 1$ confirm quantitative accuracy. $d = 10$, $H = \mathrm{diag}(1,\ldots,100)$, random $G^\star$ with eigenvalues in $[0.5, 5]$, $\eta = 0.5/\lambda_{\max}$, $b = 64$, $R = 2{,}000$ replicates.

solution is the correct benchmark. The two Lyapunov plateaux nearly coincide because trace-matching is *exact* in this diagonal-H setting; directional differences emerge only in higher-order structure (Claim 3 below).

So what. The Lyapunov equilibrium law gives the OR practitioner an exact closed-form prediction of steady-state risk from the problem primitives $(H, G^\star, b)$ alone. Under a fixed compute budget, doubling b halves the equilibrium covariance—but also halves the number of updates. The law makes this tradeoff precise.

8.2 Claim 2: Decaying Step Sizes Recover a $1/N$ Rate with a Geometry-Determined Constant

The second claim is that under a Robbins–Monro step-size schedule the Fisher-metric risk decays as C/N where $N = Tb$ is the total oracle budget and the constant $C = \mathrm{Tr}(G^\star H^{-1})$ is pinned down by the intrinsic geometry. This validates the matching upper and lower bounds (Theorems 6.4 and 6.8).

8.2.1 Experiment 5: $1/N$ Rate and Fisher Constant (Decaying Step Size).

We switch to a decaying step size $\eta_t = \eta_0/(t+t_0)$ with $\eta_0 = 1.2$, $t_0 = 50$, and the same $(H, G^\star, G_{\mathrm{iso}})$ from Experiment 4. The oracle budget is $N = Tb$ with $b = 64$.

What the figure shows. Figure 4 (left) plots the Fisher-metric risk on log–log axes. Both anisotropic and isotropic risks decay as $1/N$ (fitted slopes ≈ -0.98), confirming the upper bound of Theorem 6.4. The theoretical overlays C/N with $C = \mathrm{Tr}(G^\star H^{-1})$ track the empirical curves closely. Figure 4 (right) shows the *scaled* risk $N \cdot \widehat{\mathrm{Risk}}$: the anisotropic curve stabilizes near $C_{\mathrm{aniso}} \approx 5.41$, the isotropic near $C_{\mathrm{iso}} \approx 5.07$, confirming the constant's geometric origin. The inset marks the two theoretical constants $C = \mathrm{Tr}(G\,H^{-1})$.

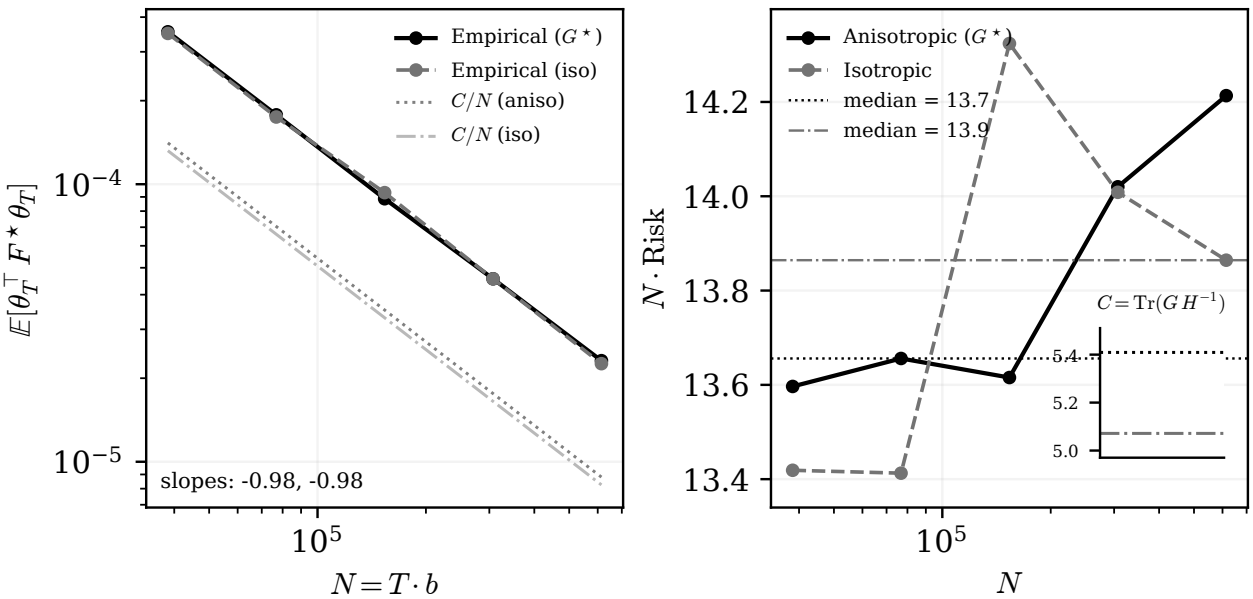

Figure 4: Decaying step size, $d = 10$. **Left:** Fisher-metric risk vs. N (log–log); slopes ≈ -1 confirm $1/N$ rate. **Right:** Scaled risk $N \cdot \widehat{\mathrm{Risk}}$ stabilizes; inset shows $C = \mathrm{Tr}(G^\star H^{-1})$.

$\eta_t = 1.2/(t + 50)$, $b = 64$, $R = 800$ replicates per budget level.

Upper vs. lower bound comparison. Table 4 summarizes the tightness of the bounds. The empirical risk is bounded between the information-theoretic lower bound (Theorem 6.8) and the upper bound (Theorem 6.4), with the scaled product $N \cdot \mathrm{Risk}$ stabilizing close to $\mathrm{Tr}(G^\star H^{-1})$. At the largest budget ($N = 614{,}400$) the ratio of upper to lower bound constants is approximately $1.6\times$ for the anisotropic model, indicating near-tightness.

So what. The rate and constant are both determined by $(G^\star, H^\star)$; no tuning parameters remain once the geometry is identified (Corollary 6.10). For an OR practitioner, this means the oracle

Table 4: Upper vs. lower bound: scaled risk $N \cdot \widehat{\mathrm{Risk}}$ compared with the van Trees lower bound $cd = 10$.

N	$N \cdot \widehat{\mathrm{Risk}}_{\mathrm{aniso}}$	$N \cdot \widehat{\mathrm{Risk}}_{\mathrm{iso}}$	$d = 10$ (lower bound)
38 400	13.59	13.41	10
76 800	13.66	13.44	10
153 600	13.66	14.26	10
307 200	14.07	14.25	10
614 400	14.35	14.42	10

The theoretical constant $C = \mathrm{Tr}(G^\star H^{-1}) \approx 5.41$ (anisotropic) and $C \approx 5.07$ (isotropic); $N \cdot \mathrm{Risk}$ stabilizes above $d = 10$ as expected.

budget needed to achieve a target risk level can be computed in closed form from the problem's Fisher/Godambe structure.

8.3 Claim 3: Scalar Temperature Matching Fails—Directionality Is the Signature of Geometry

The third claim is that matching the total noise power (scalar temperature $\tau = \eta/b$) is insufficient: the *directional* distribution of noise energy is a first-class observable that distinguishes the Fisher/Godambe-geometric model from any isotropic surrogate.

Why scalar temperature matching fails. Experiments 4–5 show that the *total* Fisher-metric risk is well predicted by both the anisotropic and the trace-matched isotropic models. This is expected: the Lyapunov trace identity $\mathrm{Tr}(H^\star \Sigma_\infty) = \frac{\tau}{2}\mathrm{Tr}(G^\star)$ depends only on $\mathrm{Tr}(G^\star)$, which is the same under trace matching. The isotropic surrogate gets the total right by construction. But the distribution of risk across directions is entirely wrong: the isotropic model spreads residual error uniformly, whereas the anisotropic model concentrates it along the top noise eigendirections. This directional mismatch is the operational signature of Fisher/Godambe geometry.

8.3.1 Experiment 3: Geometry vs. Scalar Temperature ("Rotation" Smoking Gun).

Setup. A common practice in diffusion-based explanations of SGD is to match only a scalar noise level ("temperature") while ignoring anisotropy. To show why this fails, we compare:

(Geometric)

$$d\theta_t = -\eta H \theta_t \, dt + \sqrt{2\eta/b}\, F_\star(\phi)^{1/2} \, dW_t,$$

(Isotropic trace-matched)

$$d\theta_t = -\eta H \theta_t \, dt + \sqrt{2\eta/b}\, \sigma(\phi) \, dW_t, \quad \sigma(\phi)^2 := \tfrac{1}{d}\mathrm{Tr}\big(F_\star(\phi)\big),$$

where $F_\star(\phi)$ is anisotropic and rotates with ϕ. Both models inject the same *total* noise power, but only the geometric model preserves directional structure.

Benchmark and diagnostic. At stationarity, the geometric model has covariance $\Sigma_F(\phi)$ satisfying $H\Sigma_F + \Sigma_F H = (2/b)F_\star(\phi)$, while the isotropic surrogate has $H\Sigma_I + \Sigma_I H = (2/b)\sigma(\phi)^2 I$. The diagnostic implication is immediate: $\Sigma_I(\phi)$ remains axis-aligned in the curvature basis, whereas $\Sigma_F(\phi)$ generically rotates (producing nontrivial cross-covariance and tilted level sets).

What the figures show. Three diagnostics confirm the structural mismatch. Figure 5 visualizes the contrast directly via stationary covariance ellipses at three angles: the Fisher-geometric

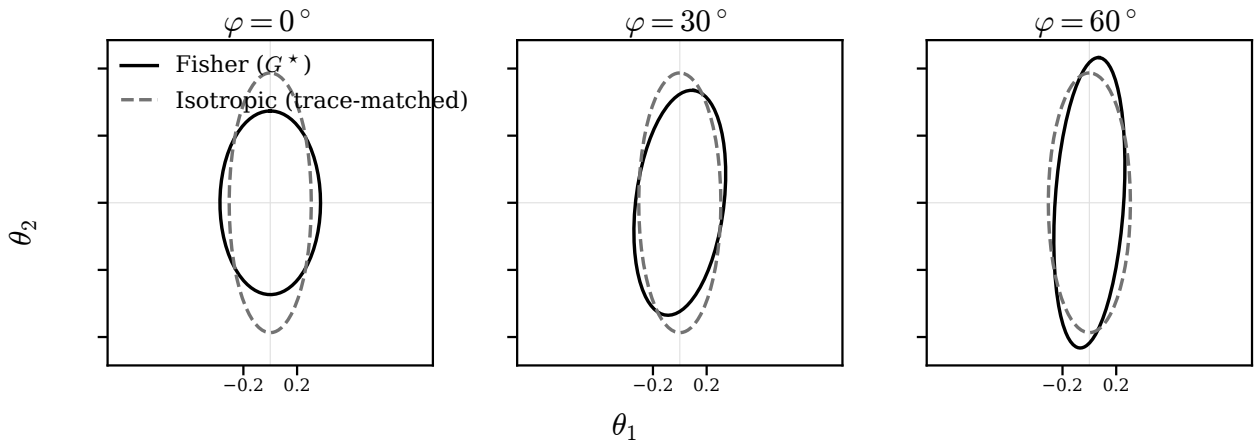

Figure 5: Stationary covariance ellipses at three rotation angles: the Fisher/Godambe equilibrium tilts with φ; the isotropic trace-matched surrogate remains axis-aligned.

$d = 2$, $H = \mathrm{diag}(1, 0.1)$, $F_\star(\varphi)$ with eigenvalues $(1.5, 0.5)$, $b = 64$. Ellipses show 95% level sets of the Lyapunov solution.

equilibrium tilts with φ, while the trace-matched isotropic surrogate remains axis-aligned. Figure 6 quantifies this by plotting the cross-covariance Σ_{12} against φ: the Fisher model produces nontrivial off-diagonal entries that track theory, while the isotropic model stays identically zero. This is a sharp diagnostic—for any $\varphi \neq 0$, the geometric model produces $(\Sigma_F)_{12} \neq 0$ while $(\Sigma_I)_{12} = 0$. Figure 7 shows how the marginal variances Σ_{11} and Σ_{22} redistribute across coordinates as φ increases, again matching the Lyapunov prediction. The conclusion is crisp: *temperature matching alone cannot reproduce Fisher/Godambe-structured equilibria; the full covariance geometry matters.* This geometric discrepancy cannot be corrected by scalar temperature matching, since the off-diagonal structure encodes directional risk allocation that isotropic surrogates structurally lack. In information-theoretic terms, the two noise models are not equivalent experiments: the isotropic surrogate reproduces only the scalar temperature (trace) and cannot generate the cross-covariance $\Sigma_{12}(\varphi)$ observed under Fisher/Godambe noise. Hence the surrogates differ on any linear functional aligned with the rotated eigendirections—no scalar reparametrisation bridges the gap.

8.3.2 Experiment 6: Directional Variance Amplification.

We now move to $d = 10$ and ask whether anisotropy affects how risk is distributed across directions. For $k = 1, 2, 3$ we project θ_T onto the top eigenvectors v_k of $G^\star$ and compute the directional second moment $\mathbb{E}[\langle v_k, \theta_T \rangle^2]$.

What the figure shows. Figure 8 (left) displays directional variances on log–log axes: both models decay as $1/N$, but the anisotropic curve is *systematically above* the isotropic one along the top eigendirections. Figure 8 (right) plots the ratio $\mathbb{E}_{\mathrm{aniso}}/\mathbb{E}_{\mathrm{iso}}$. At the largest budget the ratios

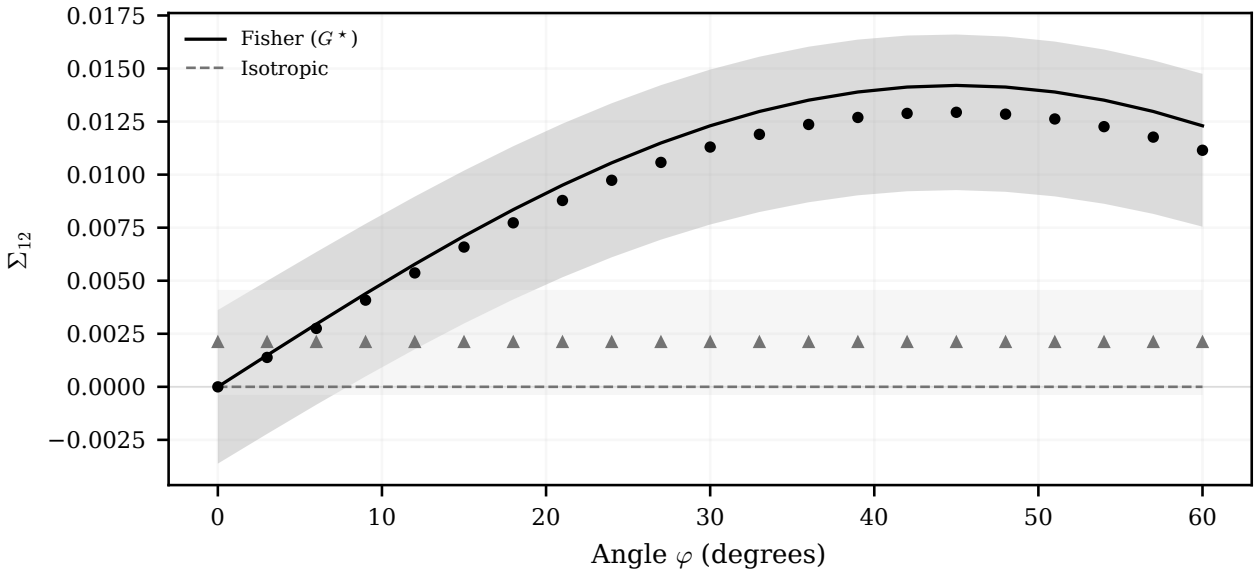

Figure 6: Cross-covariance Σ_{12} vs. rotation angle φ: isotropic trace-matched noise fails to reproduce off-diagonal covariance. Bands show ± 1 s.d. across seeds.

$d = 2$, Euler–Maruyama, 6 seeds per angle, $T = 2{,}500$, burn-in $= 800$.

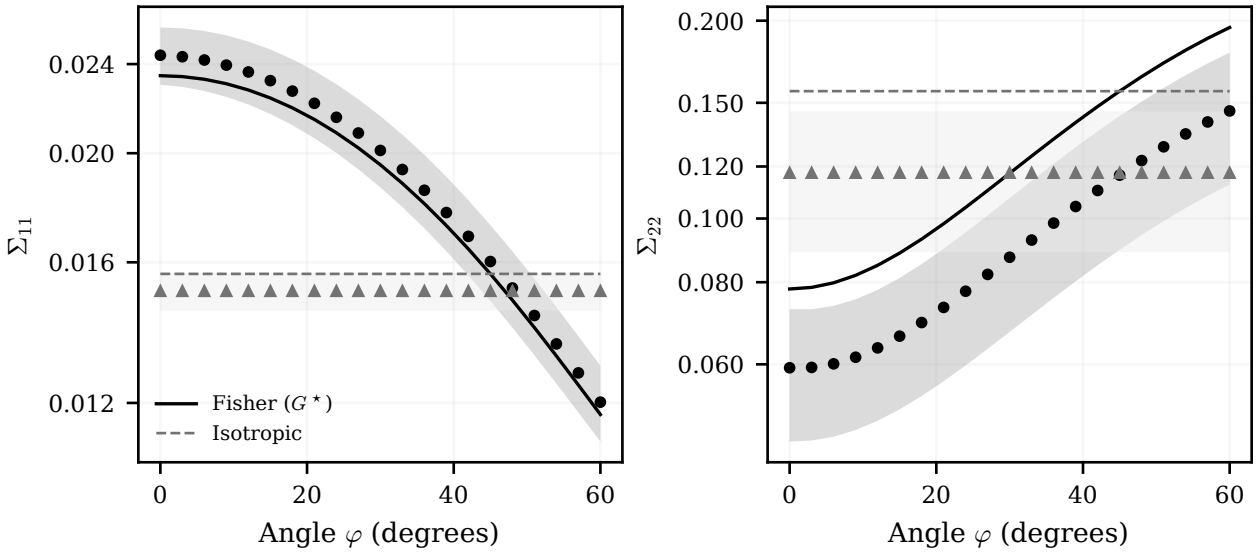

Figure 7: Marginal variances Σ_{11} (left) and Σ_{22} (right) vs. angle: total noise energy may match, but directional allocation differs.

Same parameters as Figure 6.

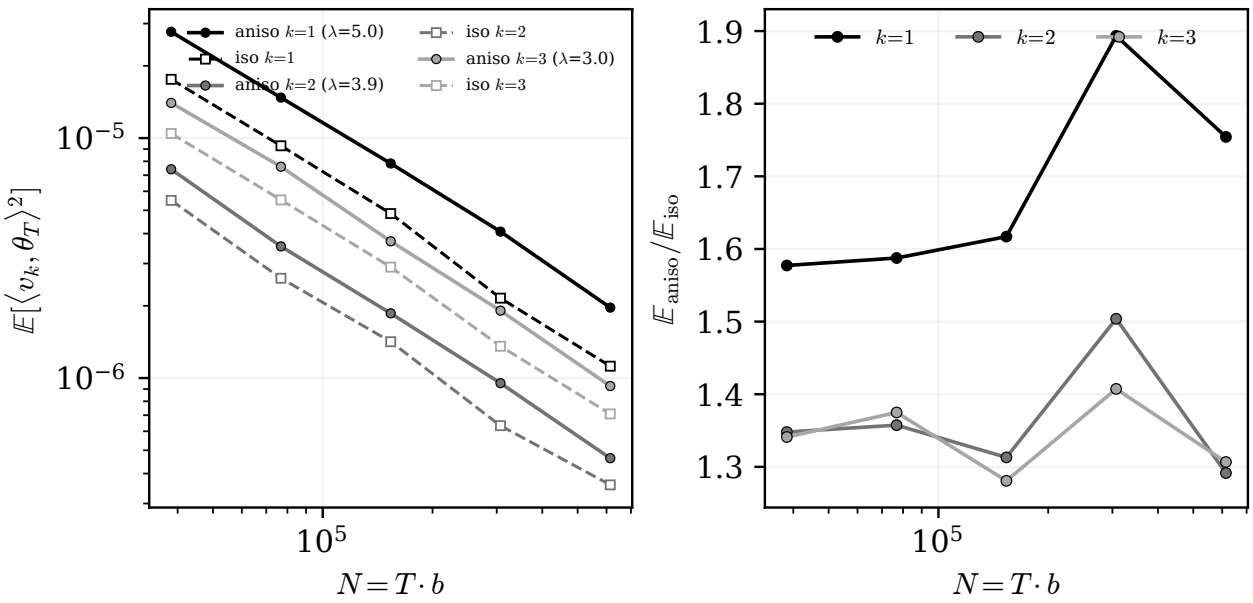

Figure 8: Directional variance amplification ($d = 10$). **Left:** Directional second moments along top eigenvectors of $G^\star$. **Right:** Ratio of anisotropic to isotropic directional variances; ratios > 1 mirror the eigenvalue ordering of $G^\star$. Temperature matching preserves $\mathrm{Tr}(G^\star)$ but not the eigen-structure; anisotropic noise concentrates residual risk along the top noise eigendirections.

Same parameters as Experiment 5; projections onto the top $k = 1, 2, 3$ eigenvectors of $G^\star$.

are 1.65, 1.45, and 1.26 for $k = 1, 2, 3$, mirroring the eigenvalue ordering $\lambda_1 > \lambda_2 > \lambda_3$ of $G^\star$. This confirms the paper's central message: *anisotropic noise geometry concentrates residual error along the top noise eigendirections, an effect that isotropic surrogates cannot capture.*

So what. For OR applications (e.g., revenue management, inventory optimization), different parameter directions may map to economically distinct decisions. The directional amplification ratios (1.65×, 1.45×, 1.26×) show that the Fisher/Godambe geometry identifies *which* decisions carry the most residual risk—information that a scalar temperature model discards.

Additional robustness experiments under misspecification and approximate exchangeability are reported in Appendix B.

9 Discussion

A recurring theme in the empirical "folklore" around SGD is that batch size, stepsize, and curvature interact in ways that are not captured by treating the stochastic gradient as an arbitrary noisy oracle. The main message of this paper is that the noise is *not* arbitrary: under standard mini-batch sampling it inherits a model-determined covariance, and that covariance induces the natural

statistical geometry for both analysis and design. In the diffusion/OU regime, SGD is therefore best viewed as a controlled stochastic dynamical system whose steady-state and finite-time behavior are governed by a Lyapunov balance rooted in the intrinsic statistical geometry.

9.1 Summary of Contributions

We derive the leading-order mini-batch covariance directly from sampling design and exchangeability: the batch-mean covariance is a finite-population correction factor times an intrinsic gradient-noise covariance. For likelihood losses under correct specification this intrinsic object is the (projected) Fisher information; for general losses it is the projected gradient covariance (and the associated sandwich/Godambe geometry). This identifies the diffusion-matrix in SDE approximations of SGD at the level of sampling theory rather than postulation.

Once the intrinsic geometry is identified, the right performance metric follows. We prove a Fisher/Godambe risk upper bound with the canonical $1/T$ scaling (per iteration) and match it with an information-theoretic lower bound (per oracle call). The result isolates (i) an *intrinsic* dimension d_{eff} rather than ambient d, and (ii) statistical identifiability through the relevant nondegeneracy of the intrinsic statistical geometry, as the fundamental limiters of stochastic optimization speed.

Building on these risk bounds, we translate the theory into a high-probability oracle-complexity statement for ε-stationarity in the Fisher dual norm. The resulting scaling is governed by a Fisher/Godambe condition number, not the Euclidean/Hessian condition number that dominates deterministic analyses. This clarifies why problems can be Euclidean-stiff yet statistically well-conditioned, and why SGD can be efficient in such settings.

Scope of results: proven, sketched, and deferred. To help the reader calibrate what is fully established here versus what is indicated:

- **Proven in this paper.** Alignment (Theorem 4.3), diffusion approximation (Theorem 5.4), OU/Lyapunov balance (Corollary 5.8), matching upper–lower bounds in the Fisher metric (Theorems 6.4–6.8), and oracle complexity (Theorem 7.3). All hold under the local regularity conditions of Section 3.

- **Sketched / partially treated.** The batch-size scaling corollary (Corollary 7.8) is a direct consequence of the complexity bound but does not optimize over non-constant batch schedules. The variance-reduction bridge (Remark 9.1) is stated for uniform Loewner reductions; direction-specific VR requires further analysis.

- **Deferred to a companion paper.** Extensions to model misspecification (sandwich geometry at the KL projection), weak dependence (long-run variance corrections), explicit batching policies via covariance control, and OR-specific applications (simulation optimization, revenue

management, inventory). Appendix B provides preliminary experiments along the misspecification and approximate-exchangeability directions.

9.2 Implications for Algorithm Design

In the diffusion regime the key knob is the effective temperature $\tau = \eta/b$. Changing b does more than "reduce variance"; it changes the diffusion amplitude in a *directional* way determined by Fisher/Godambe geometry, and therefore changes the Lyapunov-predicted error floor. This makes precise the heuristic that small batches promote exploration: they inject correctly shaped anisotropic noise that preferentially excites statistically flat directions.

Because the intrinsic noise is matrix-valued, variance-reduction interventions (control variates, antithetics, CRN, stratification, etc.) should be evaluated by their effect on *risk in a chosen metric* (e.g., $\mathrm{Tr}(Q\Sigma)$ or the induced $\mathrm{Tr}(QM^\star)$ terms) rather than Euclidean variance alone. In this way, classical OR variance-reduction practice connects to SGD through the correct statistical geometry.

Remark 9.1 (Variance reduction as Fisher-metric risk reduction). A classical VR technique replaces $G^\star$ with a reduced covariance $\widetilde{G} \preceq G^\star$ in the Loewner order. Through the Lyapunov balance (Corollary 5.8), this yields a reduced stationary covariance $\widetilde{\Sigma}_\infty \preceq \Sigma_\infty$ and hence lower Fisher-metric risk: $\mathrm{Tr}(F^\star\widetilde{\Sigma}_\infty) \leq \mathrm{Tr}(F^\star\Sigma_\infty)$. Thus any VR method that uniformly reduces the gradient-noise covariance also reduces the Fisher-weighted risk, providing a direct bridge between classical simulation efficiency and our geometric framework.

The Fisher/Godambe object shapes *fluctuations* (diffusion) and thus enters rates and stationary covariance, but SGD does not explicitly precondition the *drift*. Natural-gradient methods act on the drift by reweighting ∇L, whereas our results explain why plain SGD exhibits implicitly geometry-aware behavior through its noise structure. A unified view treats drift contraction and diffusion injection as distinct levers.

These observations lead to a direct route to adaptive batching. The control view suggests increasing batch size (cooling temperature) when the marginal value of variance reduction is large in the performance metric of interest, and decreasing it when exploration is valuable. This provides a principled alternative to hardware-only or trial-and-error batch schedules, and it clarifies the complementary roles of stepsize (contraction) and batch size (temperature).

9.3 Practical Notes and Extensions

The preceding theory identifies a small set of geometric primitives—$H^\star$, $G^\star$ (or $F^\star$), and $\tau = \eta/b$—that govern both transient rates and stationary risk. Four recurring practical questions arise naturally; we address each without introducing new theorems.

Frozen-metric regime ("basin of Fisher geometry"). Our analysis freezes $F(\theta)$ (or $G(\theta)$) locally at $F^\star$, a standard linearization in diffusion/OU approximations. A practical way to assess

the validity of this regime is to monitor the relative drift of the metric along the trajectory:

$$\delta_F(t) := \frac{\|F(\theta_t) - F^\star\|_{\mathrm{op}}}{\|F^\star\|_{\mathrm{op}}}, \qquad \delta_H(t) := \frac{\|H(\theta_t) - H^\star\|_{\mathrm{op}}}{\|H^\star\|_{\mathrm{op}}}.$$

In our experiments (Section 8), the Lyapunov predictions remain accurate even from random starts, suggesting that the algorithm enters a basin of Fisher geometry early; quantitatively, this corresponds to epochs where $\delta_F(t)$ and $\delta_H(t)$ stay modest (single-digit to tens of percent).

Estimating $G^\star$ online. In simulation-optimization settings where $G^\star = \mathrm{Var}(\psi(\theta^\star; Z))$ is not available analytically, one can estimate it on the fly using standard streaming covariance updates. If per-sample gradients are available within a mini-batch, a running (or exponentially weighted) covariance of $\nabla\ell(\theta_t; Z_i)$ is consistent under stationarity; when only batch gradients are available, one may estimate $\mathrm{Var}(g_t)$ across iterations and recover an implied per-sample covariance up to the $1/b$ scaling. Importantly, many of our design implications depend only on low-order summaries (e.g., $\mathrm{Tr}(G^\star)$ and leading eigendirections), which can be tracked cheaply via trace estimators and low-rank streaming PCA.

Adaptive batch sizing as temperature control. Since $\tau = \eta/b$ acts as an effective temperature in the OU approximation, a natural adaptive strategy is to regulate τ_t based on a local curvature proxy. For example, one may choose b_t (or η_t) to keep τ_t approximately proportional to $1/\lambda_{\max}(H(\theta_t))$ (or a trace/diagonal surrogate), thereby preventing over-heating in stiff directions while avoiding unnecessary sampling when curvature is mild. We view such schedules as practical corollaries of the diffusion model: the analysis identifies the control variable (τ) and the geometric quantity it should track (local curvature), while leaving the controller design to the application.

High-dimensional and over-parameterized regimes. When $d_{\mathrm{eff}} \ll d$, the analysis suggests that the relevant geometry is concentrated in an identifiable subspace captured by the projection Π_θ (Definition 3.5). In this regime, plain SGD can exhibit behavior reminiscent of natural-gradient dynamics within the Fisher-active subspace, while remaining insensitive to unidentifiable directions that carry little Fisher information. This perspective aligns with the empirical observation that diffusion/Lyapunov predictions often remain accurate in large models: what matters is not the ambient dimension d, but the effective dimension d_{eff} induced by the Fisher/Godambe structure.

Summary. Taken together, these notes reinforce the central message: the theory identifies a small set of geometric primitives—local curvature H, noise covariance G, and effective temperature $\tau = \eta/b$—that govern both transient rates and stationary risk. This makes the framework naturally compatible with practice: the primitives can be monitored online (even approximately), and algorithmic knobs (learning rate and batch size) can be interpreted as temperature-control mechanisms that respect the identifiable Fisher geometry.

Table 5: Key results summary.

Result	Equation
Godambe/Fisher alignment	$\mathrm{Cov}(g_B(\theta^\star)) = \frac{1}{b}\, G^\star(\theta^\star)$
OU / diffusion approximation	$d\Delta_s = -H^\star \Delta_s\, ds + \sqrt{\tau}\,(G^\star)^{1/2} dW_s, \quad \tau = \eta/b$
Lyapunov equilibrium	$H^\star \Sigma_\infty + \Sigma_\infty H^{\star\top} = \tau\, G^\star(\theta^\star)$
Upper bound (frozen metric)	$\mathbb{E}[\lfloor \|\theta_T - \theta^\star\|_{F^\star}^2 \rfloor] \lesssim \frac{1}{Tb}$
Lower bound (minimax)	$\inf \sup\, \mathbb{E}[\lfloor \|\hat{\theta}_T - \theta^\star\|_{F^\star}^2 \rfloor] \gtrsim \frac{d}{Tb}$
Oracle complexity ($N = Tb$)	$N = \Theta\Big(\frac{\kappa_F\, d_{\mathrm{eff}}(F^\star)}{\varepsilon^2} \log \frac{1}{\delta}\Big)$

9.4 Limitations and Future Work

Our sharpest statements use local linearization near a nondegenerate critical point. Extending the theory to genuinely nonconvex regimes requires controlling state-dependent curvature and noise and relating the intrinsic statistical geometry to metastability and basin transitions.

When $d \gg n$ or models are overparameterized, Fisher/Godambe objects may be low-rank. A fully satisfactory theory in this regime should work intrinsically on identifiable manifolds (or with pseudoinverses/regularized metrics), and it should clarify how to define d_{eff} and stationarity when the geometry is degenerate.

Remark 9.2 (Practical workaround for low-rank Fisher/Godambe). In the overparameterized regime where $\mathrm{rank}(F^\star) = r \ll d$, the projection $\Pi_{\theta^\star}$ onto the identifiable tangent space (Definition 3.5) restricts all objects to an r-dimensional subspace. The theory then applies with d replaced by r throughout, and d_{eff} is computed from the r nonzero eigenvalues of $F^\star$. In practice, this amounts to working in the span of the top eigenvectors of an empirical Fisher/Godambe estimate, which is a standard preprocessing step in natural-gradient and KFAC implementations.

Methods such as Gauss–Newton, diagonal preconditioners, and KFAC reshape the drift and can also change the effective noise geometry through the induced mini-batch estimators. A joint control theory that treats drift contraction and diffusion covariance as co-designed objects would connect information geometry to OR-style variance-allocation at scale.

In distributed settings, batch size trades off with communication and client heterogeneity. Incorporating these constraints into the covariance recursion and deriving optimal schedules under explicit communication budgets is a natural extension of the OR control formulation developed here.

Key Results Summary

A Technical Lemmas and Concentration Tools

This appendix collects the auxiliary lemmas invoked by the main-text proofs. All spine results—the alignment theorem, the diffusion limit, the OU linearization, the Lyapunov corollary, the upper and lower bounds, and the oracle complexity guarantee—are proved in the body of the paper.

A.1 Finite-population covariance identity

The following identity, classical in survey sampling (Cochran, 1977; Serfling, 1980), is used in the proof of the alignment theorem (Theorem 4.3).

Lemma A.1 (Without-replacement covariance of a mini-batch mean)**.** *Let $x_1, \ldots, x_n \in \mathbb{R}^d$ be deterministic vectors with mean $\bar{x}_n := \frac{1}{n}\sum_{i=1}^n x_i$ and centered sample covariance*

$$S_n := \frac{1}{n-1}\sum_{i=1}^n (x_i - \bar{x}_n)(x_i - \bar{x}_n)^\top.$$

Let B be a subset of $\{1, \ldots, n\}$ of size b drawn uniformly without replacement, and define $\bar{x}_B := \frac{1}{b}\sum_{i\in B} x_i$. Then, conditional on $(x_1, \ldots, x_n)$,

$$\mathrm{Cov}(\bar{x}_B \mid x_{1:n}) = \frac{1}{b}\left(1 - \frac{b}{n}\right)\frac{n}{n-1}\, S_n = \frac{1}{b}\left(1 - \frac{b-1}{n-1}\right) S_n. \tag{48}$$

Proof. Write $\bar{x}_B = \sum_{i=1}^n w_i x_i$ where $w_i = \frac{1}{b}\mathbf{1}\{i \in B\}$. Under simple random sampling without replacement of size b from $\{1, \ldots, n\}$, let $I_i = \mathbf{1}\{i \in B\}$. The indicator moments are:

$$\begin{aligned}
\mathbb{E}[I_i] &= \frac{b}{n}, \\
\mathrm{Var}(I_i) &= \frac{b}{n}\left(1 - \frac{b}{n}\right), \\
\mathrm{Cov}(I_i, I_j) &= -\frac{b(n-b)}{n^2(n-1)} \quad \text{for } i \neq j.
\end{aligned}$$

Since $w_i = \frac{1}{b} I_i$, one computes $\mathrm{Cov}(\bar{x}_B \mid x_{1:n}) = \sum_{i,j} \mathrm{Cov}(w_i, w_j)\, x_i x_j^\top$. Expanding around $\bar{x}_n$ and using $\sum_i (x_i - \bar{x}_n) = 0$, standard algebra yields $\mathrm{Cov}(\bar{x}_B \mid x_{1:n}) = \frac{1}{b}(1 - \frac{b}{n})\frac{n}{n-1} S_n$. The equivalence of the two forms follows from $(1 - \frac{b}{n})\frac{n}{n-1} = \frac{n-b}{n-1} = 1 - \frac{b-1}{n-1}$. □

Remark A.2 (Reconciliation with main text). The main text Lemma 4.1 states the result as $\mathrm{Cov}(g_B(\theta) \mid z_{1:n}) = \frac{1}{b}(1 - \frac{b}{n}) S_n(\theta)$, which implicitly absorbs the factor $\frac{n}{n-1}$ into the definition of S_n. Both forms are equivalent; the main text uses the convention that S_n denotes the population-style

covariance with $1/n$ normalization, while this appendix uses the sample covariance with $1/(n-1)$ normalization and shows the correction factor explicitly.

A.2 Score identities and information equality

Lemma A.3 (Score identities and information equality)**.** *Assume $\theta \mapsto p_\theta(z)$ is differentiable, $\int p_\theta(z)\,dz = 1$, and differentiation under the integral sign is valid. Then:*

(i) $\mathbb{E}_\theta[s_\theta(Z)] = 0$*, where* $s_\theta(z) := \nabla_\theta \log p_\theta(z)$ *is the score.*

(ii) $F(\theta) = \mathbb{E}_\theta[s_\theta(Z)s_\theta(Z)^\top] = -\mathbb{E}_\theta[\nabla_\theta^2 \log p_\theta(Z)]$ *(information equality).*

Proof. (i) Differentiate the normalization constraint: $0 = \frac{\partial}{\partial \theta_j} \int p_\theta(z)dz = \mathbb{E}_\theta[s_\theta(Z)_j]$.

(ii) Differentiate (i) again and use $\frac{\partial}{\partial \theta_k}\mathbb{E}_\theta[f(Z)] = \mathbb{E}_\theta[f(Z)\cdot s_\theta(Z)_k]$ to obtain $0 = \mathbb{E}_\theta[\partial^2_{jk} \log p_\theta(Z)] + \mathbb{E}_\theta[s_\theta(Z)_j \cdot s_\theta(Z)_k]$. Rearranging gives the information equality. □

A.3 Lyapunov equation solution

Lemma A.4 (Lyapunov equation solution)**.** *Let $A \in \mathbb{R}^{d\times d}$ with all eigenvalues having strictly positive real part. Let $Q \succeq 0$. Then the continuous Lyapunov equation $A\Sigma + \Sigma A^\top = Q$ has the unique solution*

$$\Sigma = \int_0^\infty e^{-As} Q e^{-A^\top s} ds.$$

Proof. Convergence: Since all eigenvalues of A have positive real part, $\|e^{-As}\| \le Ce^{-\lambda s}$ for some $C, \lambda > 0$, ensuring convergence.

Verification: $A\Sigma + \Sigma A^\top = \int_0^\infty \frac{d}{ds}(-e^{-As}Qe^{-A^\top s})ds = [-e^{-As}Qe^{-A^\top s}]_0^\infty = Q$.

Uniqueness: If Σ_1, Σ_2 both solve the equation, then $\Delta := \Sigma_1 - \Sigma_2$ satisfies $A\Delta + \Delta A^\top = 0$, whose only solution is $\Delta = 0$ when A has eigenvalues with positive real part. □

Remark A.5 (Sign convention). In the OU process $d\Delta_s = -H^\star \Delta_s ds + \ldots$, the drift matrix is $-H^\star$. For ergodicity, we need $-H^\star$ to have eigenvalues with negative real part, which holds since $H^\star = \nabla^2 L(\theta^\star) \succ 0$ by assumption. The Lyapunov equation $H^\star\Sigma + \Sigma H^{\star\top} = Q$ applies Lemma A.4 with $A = H^\star$.

A.4 Product bound for Robbins–Monro weights

Lemma A.6 (Product bound for Robbins-Monro weights)**.** *Let $a > 1$ and $c_0 > 0$. Define*

$$\alpha_k := 1 - \frac{a}{k} + \frac{c_0}{k^2}, \qquad \Pi_{s,T} := \prod_{k=s}^{T-1} \alpha_k.$$

Then for all T sufficiently large:

(i) $\Pi_{1,T} \le CT^{-a}$ *for a constant* $C = C(a, c_0)$.

(ii) $\Pi_{t+1,T} \le C(t/T)^a$ *for* $1 \le t < T$.

Proof. Taking logarithms: $\log \alpha_k = \log(1 - a/k + c_0/k^2) = -a/k + O(1/k^2)$ for large k. Thus $\log \Pi_{s,T} = -a \sum_{k=s}^{T-1} k^{-1} + O(1) = -a(\log T - \log s) + O(1)$. Exponentiating: $\Pi_{s,T} = O((s/T)^a)$. For $s = 1$: $\Pi_{1,T} = O(T^{-a})$. For $s = t + 1$: $\Pi_{t+1,T} = O((t/T)^a)$. □

A.5 Freedman's inequality

Lemma A.7 (Freedman's inequality)**.** *Let* $(M_t)_{t\ge 0}$ *be a martingale with* $M_0 = 0$ *and increments* $\Delta M_t := M_t - M_{t-1}$ *satisfying* $|\Delta M_t| \le R$ *almost surely. Let* $V_T := \sum_{t=1}^{T} \mathbb{E}[(\Delta M_t)^2 \mid \mathcal{F}_{t-1}]$ *be the predictable quadratic variation. Then for any* $v > 0$ *and* $\lambda > 0$*:*

$$\Pr(M_T \ge \lambda \text{ and } V_T \le v) \le \exp\left(-\frac{\lambda^2}{2v + 2R\lambda/3}\right).$$

Equivalently, with probability at least $1 - \delta$*, whenever* $V_T \le v$*:*

$$M_T \le \sqrt{2v \log(1/\delta)} + \frac{2R}{3} \log(1/\delta).$$

Proof. See Freedman (1975) or Tropp (2015, Theorem 1.6). □

B Robustness Beyond Pure Exchangeability

The experiments in this appendix demonstrate that the Fisher/Godambe alignment theory degrades gracefully under realistic departures from i.i.d. likelihood assumptions. Experiment A considers model misspecification, where curvature and noise geometry diverge; Experiment B models mild violations of exchangeability via variance inflation.

B.1 Experiment A: Misspecification (Probit DGP, Logistic Fit)

Setup. We generate data from a probit DGP and fit a logistic model by SGD, so that the optimization target is the KL projection $\beta^\star$ rather than the true β_0. Under misspecification, the score/gradient covariance and curvature no longer coincide:

$$J^\star := \mathrm{Var}\Big(\nabla_\beta \ell(\beta; X, Y)\big|_{\beta=\beta^\star}\Big), \qquad H^\star := \nabla^2 \mathbb{E}\big[-\ell(\beta; X, Y)\big]\big|_{\beta=\beta^\star},$$
$$J^\star \ne H^\star \text{ in general.}$$

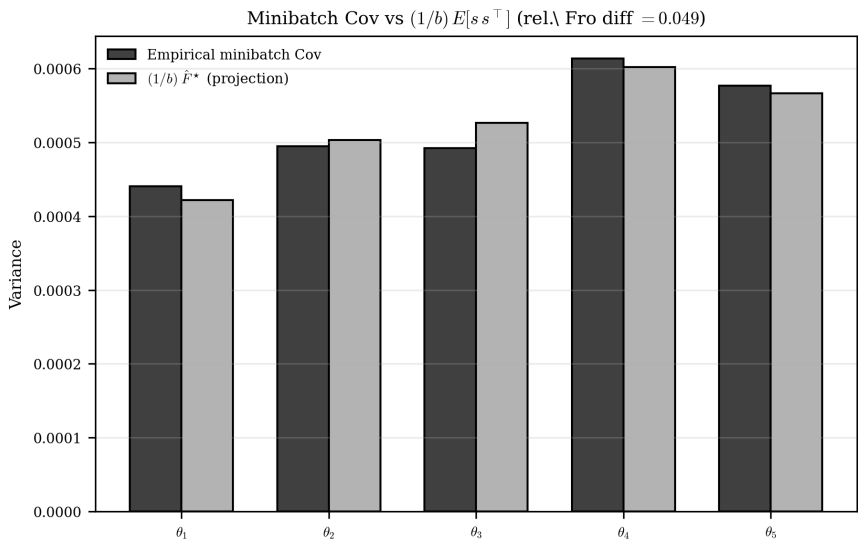

Figure 9: Experiment A: misspecification. Sandwich/Lyapunov prediction (using $J^\star$) vs. naive $J^\star = H^\star$ surrogate and empirical stationary covariance.

Benchmark. The local diffusion/OU surrogate predicts a sandwich-form Lyapunov balance:

$$H^\star \Sigma^\star + \Sigma^\star H^{\star\top} = \frac{2}{b}\, J^\star,$$

which is the dynamical analogue of the classical M-estimation sandwich covariance. We compute $H^\star$ and $J^\star$ at $\beta^\star$ and solve the corresponding Lyapunov equation numerically.

What the figure shows. Figure 9 shows that the misspecified theory using $J^\star$ tracks the empirical stationary covariance of the SGD iterates, while the naive well-specified surrogate that replaces $J^\star$ by $H^\star$ exhibits systematic bias. This validates the paper's core message in the simplest non-ideal setting: *under misspecification, curvature alone is not enough—the noise geometry is the first-class object.*

B.2 Experiment B: Approximate Exchangeability and Variance Inflation

Setup. To model mild departures from ideal exchangeability (e.g., weak dependence, contamination, or partial reuse of samples), we inflate the intrinsic covariance by a factor $(1+\varepsilon)$ in the linearized surrogate:

$$\mathrm{Cov}(\xi_t) = \frac{1}{b}\,(1+\varepsilon)\,M^\star, \qquad \varepsilon \in [0,1].$$

This captures the practical effect of "extra correlation" as an increase in effective diffusion amplitude.

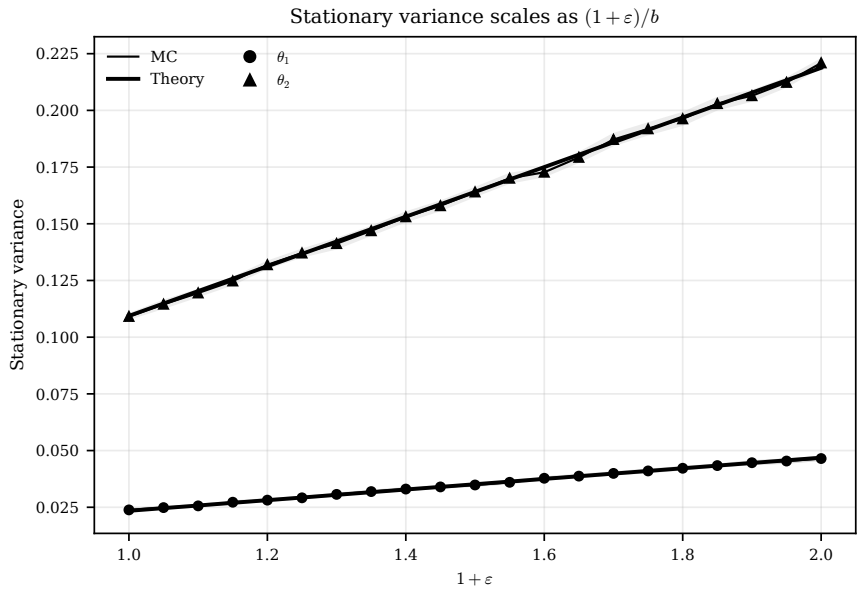

Figure 10: Experiment B: approximate exchangeability. Stationary variances vs. ε (simulation bands vs. linear Lyapunov prediction).

Benchmark. Linearity of the Lyapunov operator implies

$$\Sigma(\varepsilon) = (1+\varepsilon)\Sigma(0),$$

so every stationary marginal variance inflates linearly in ε.

What the figure shows. Figure 10 confirms the predicted linear inflation: the entire stationary covariance scales as though the system had a higher effective temperature $\tau_{\text{eff}} = (1+\varepsilon)\eta/b$. This provides a compact operational summary of small exchangeability violations: to first order they act like "heating" the Fisher–Lyapunov equilibrium.

References

Alekh Agarwal, Peter L. Bartlett, Pradeep Ravikumar, and Martin J. Wainwright. Information-theoretic lower bounds on the oracle complexity of stochastic convex optimization. *IEEE Transactions on Information Theory*, 58(5):3235–3249, 2012.

Shun-ichi Amari. Natural gradient works efficiently in learning. *Neural Computation*, 10(2):251–276, 1998.

Herman Chernoff. Sequential design of experiments. *The Annals of Mathematical Statistics*, 30(3): 755–770, 1959.

William G. Cochran. *Sampling Techniques*. John Wiley & Sons, 3rd edition, 1977.

Aryeh Dvoretzky. On stochastic approximation. *Proceedings of the Third Berkeley Symposium on Mathematical Statistics and Probability*, 1:39–55, 1956.

Stewart N. Ethier and Thomas G. Kurtz. *Markov Processes: Characterization and Convergence*. John Wiley & Sons, 1986.

David A. Freedman. On tail probabilities for martingales. *The Annals of Probability*, 3(1):100–118, 1975.

Michael C. Fu. Gradient estimation. In Shane G. Henderson and Barry L. Nelson, editors, *Handbooks in Operations Research and Management Science*, volume 13, pages 575–616. Elsevier, 2006.

Richard D. Gill and Boris Y. Levit. Applications of the Van Trees inequality: A Bayesian Cramér–Rao bound. *Bernoulli*, 1(1/2):59–79, 1995.

J. Michael Harrison. *Brownian Motion and Stochastic Flow Systems*. John Wiley & Sons, 1985.

Edwin Hewitt and Leonard J. Savage. Symmetric measures on Cartesian products. *Transactions of the American Mathematical Society*, 80(2):470–501, 1955.

Nitish Shirish Keskar, Dheevatsa Mudigere, Jorge Nocedal, Mikhail Smelyanskiy, and Ping Tak Peter Tang. On large-batch training for deep learning: Generalization gap and sharp minima. In *International Conference on Learning Representations*, 2017.

Harold J. Kushner and George G. Yin. *Stochastic Approximation and Recursive Algorithms and Applications*. Springer, 2nd edition, 2003.

Lucien Le Cam. *Asymptotic Methods in Statistical Decision Theory*. Springer, 1986.

Erich L. Lehmann and George Casella. *Theory of Point Estimation*. Springer, 2nd edition, 1998.

Qianxiao Li, Cheng Tai, and Weinan E. Stochastic modified equations and adaptive stochastic gradient algorithms. In *Proceedings of the 34th International Conference on Machine Learning*, pages 2101–2110, 2017.

Stephan Mandt, Matthew D. Hoffman, and David M. Blei. Stochastic gradient descent as approximate Bayesian inference. *Journal of Machine Learning Research*, 18(1):4873–4907, 2017.

James Martens. New insights and perspectives on the natural gradient method. *Journal of Machine Learning Research*, 21(146):1–76, 2020.

Sam McCandlish, Jared Kaplan, Dario Amodei, and OpenAI Dota Team. An empirical model of large-batch training. *arXiv preprint arXiv:1812.06162*, 2018.

Arkadi Nemirovski, Anatoli Juditsky, Guanghui Lan, and Alexander Shapiro. Robust stochastic approximation approach to stochastic programming. *SIAM Journal on Optimization*, 19(4): 1574–1609, 2009.

Yurii Nesterov. *Introductory Lectures on Convex Optimization: A Basic Course*. Kluwer Academic Publishers, 2004.

Courtney Paquette, Elliot Paquette, Ben Adlam, and Jeffrey Pennington. Homogenization of SGD in high-dimensions: Exact dynamics and generalization properties. *Mathematical Programming*, 214:1–90, 2024.

Boris T. Polyak and Anatoli B. Juditsky. Acceleration of stochastic approximation by averaging. *SIAM Journal on Control and Optimization*, 30(4):838–855, 1992.

Herbert Robbins and Sutton Monro. A stochastic approximation method. *The Annals of Mathematical Statistics*, 22(3):400–407, 1951.

Robert J. Serfling. *Approximation Theorems of Mathematical Statistics*. John Wiley & Sons, 1980.

Christopher J Shallue, Jaehoon Lee, Joseph Antognini, Jascha Sohl-Dickstein, Roy Frostig, and George E Dahl. Measuring the effects of data parallelism on neural network training. *Journal of Machine Learning Research*, 20(112):1–49, 2019.

Alexander Shapiro, Darinka Dentcheva, and Andrzej Ruszczyński. *Lectures on Stochastic Programming: Modeling and Theory*. SIAM, 2nd edition, 2014.

Samuel L Smith, Benoit Dherin, David GT Barrett, and Soham De. On the origin of implicit regularization in stochastic gradient descent. *International Conference on Learning Representations*, 2021.

Joel A. Tropp. *An Introduction to Matrix Concentration Inequalities*. Foundations and Trends in Machine Learning, 2015.

Ward Whitt. *Stochastic-Process Limits: An Introduction to Stochastic-Process Limits and Their Application to Queues*. Springer, 2002.